SANDIA REPORT
SAND2013-9787
Unlimited Release
Printed November 2013

New Composite Separator Pellet to Increase Power Density and Reduce Size of Thermal Batteries

Lisa A. Mondy, Christine C. Roberts, Anne M. Grillet, Melissa M. Soehnel, David A. Barringer, Christopher B. Diantonio, Tom Chavez, David Ingersoll, Lindsey G. Hughes, Lindsey R. Evans, Stephanie Fitchett

Prepared by
Sandia National Laboratories
Albuquerque, New Mexico 87185 and Livermore, California 94550

Sandia National Laboratories is a multi-program laboratory managed and operated by Sandia Corporation, a wholly owned subsidiary of Lockheed Martin Corporation, for the U.S. Department of Energy's National Nuclear Security Administration under contract DE-AC04-94AL85000.

Approved for public release; further dissemination unlimited.

Sandia National Laboratories

Issued by Sandia National Laboratories, operated for the United States Department of Energy by Sandia Corporation.

NOTICE: This report was prepared as an account of work sponsored by an agency of the United States Government. Neither the United States Government, nor any agency thereof, nor any of their employees, nor any of their contractors, subcontractors, or their employees, make any warranty, express or implied, or assume any legal liability or responsibility for the accuracy, completeness, or usefulness of any information, apparatus, product, or process disclosed, or represent that its use would not infringe privately owned rights. Reference herein to any specific commercial product, process, or service by trade name, trademark, manufacturer, or otherwise, does not necessarily constitute or imply its endorsement, recommendation, or favoring by the United States Government, any agency thereof, or any of their contractors or subcontractors. The views and opinions expressed herein do not necessarily state or reflect those of the United States Government, any agency thereof, or any of their contractors.

Printed in the United States of America. This report has been reproduced directly from the best available copy.

Available to DOE and DOE contractors from
U.S. Department of Energy
Office of Scientific and Technical Information
P.O. Box 62
Oak Ridge, TN 37831

Telephone: (865) 576-8401
Facsimile: (865) 576-5728
E-Mail: reports@adonis.osti.gov
Online ordering: http://www.osti.gov/bridge

Available to the public from
U.S. Department of Commerce
National Technical Information Service
5285 Port Royal Rd.
Springfield, VA 22161

Telephone: (800) 553-6847
Facsimile: (703) 605-6900
E-Mail: orders@ntis.fedworld.gov
Online order: http://www.ntis.gov/help/ordermethods.asp?loc=7-4-0#online

SAND2013-9787
Unlimited Release
Printed November 2013

New Composite Separator Pellet to Increase Power Density and Reduce Size of Thermal Batteries

Lisa A. Mondy, Christine C. Roberts, Anne M. Grillet, Melissa M. Soehnel, David A. Barringer
Thermal/ Fluid Experimental Sciences

Christopher B. Diantonio, Tom Chavez
Electronic, Optical, and Nano Materials

David Ingersoll
Advanced Power Sources R&D

Lindsey G. Hughes
Organic Materials Science

Lindsey R. Evans
Advanced Materials Laboratory

Stephanie Fitchett
Human Factors and Statistics

Sandia National Laboratories
P.O. Box 5800
Albuquerque, New Mexico 87185-MS0346

Abstract

We show that it is possible to manufacture strong macroporous ceramic films that can be backfilled with electrolyte to form rigid separator pellets suitable for use in thermal batteries. Several new ceramic manufacturing processes are developed to produce sintered magnesium oxide foams with connected porosities of over 80% by volume and with sufficient strength to withstand the battery manufacturing steps. The effects of processing parameters are quantified, and methods to imbibe electrolyte into the ceramic scaffold demonstrated. Preliminary single cell battery testing show that some of our first generation pellets exhibit longer voltage life with comparable resistance at the critical early times to that exhibited by a traditional pressed pellets. Although more development work is needed to optimize the processes to create these rigid separator pellets, the results indicate the potential of such ceramic separator pellets to be equal, if not superior to, current pressed pellets. Furthermore, they could be a replacement for critical material that is no longer available, as well as improving battery separator strength, decreasing production costs, and leading to shorter battery stacks for long-life batteries.

ACKNOWLEDGMENTS

The authors would like to acknowledge helpful discussions with Karen Waldrip and Chris Apblett (2546) and their efforts in the lab and those of Michael Russell (2546) to find the best method to backfill the ceramic foams with electrolyte. Adrian Wagner (1833) was crucial in providing laser cutting for all of our samples, some of which were very fragile and challenging to cut. Laura Biedermann (1748) helped analyze droplet diameters in the Pickering emulsions. Thanks, too, to Bion Shelden (1512) for performing TGA measurements. SEM analysis was carried out in the TEM/FIB laboratory at the University of New Mexico, Albuquerque, New Mexico. CryoSEM was performed by Chris Frethem, Characterization Facility, U Minnesota. Anodes, cathodes, and separators for single cell tests were pressed by David Herman (25481). Robert Fox (2547) also aided in single cell test execution. This work was funded under LDRD Project Number 151359 and Title "New Composite Separator Pellet to Increase Power Density and Reduce Size of Thermal Batteries".

CONTENTS

1. INTRODUCTION 11

2. GELLED MAGNESIUM OXIDE SEPARATORS 13
   2.1. Introduction 13
   2.2. Materials and Methods 13
      2.2.1. Sample Preparation 13
      2.2.2. Characterization 14
   2.3. Results 15
      2.3.1. Effect of Ball Milling and the Hydrolysis of Magnesium Oxide 15
      2.3.2. Sample Porosity 21
      2.3.3. Separator Quality 23
   2.4. Conclusions 25

3. PICKERING EMULSION MAGNESIUM OXIDE SEPARATORS 26
   3.1. Introduction 26
   3.2. Methods 26
      3.2.1. Pickering Emulsion Synthesis 26
      3.2.2. Characterization 27
   3.3. Results 28
      3.3.1. Creation of Magnesium Oxide Pickering Emulsions 28
      3.3.2. Effects of Brucite Conversion 31
      3.3.3. Effects of Material and Processing Variables on Sample Porosity 33
      3.3.4. Pickering Emulsion Separator Performance 38
   3.4. Conclusions 40

4. TRADITIONAL METHODS TO PRODUCE CERAMIC FOAMS 41
   4.1. Introduction 41
   4.2. Methods 41
      4.2.1. Producing Macroporous Reticulated Ceramic Structures Utilizing a Replica Technique 41
      4.2.2. Producing Macroporous Ceramic Structures Utilizing a Sacrificial Poreformer and Tape Casting 43
   4.3. Results 47
      4.3.1. Replication Technique 47
      4.3.2. Tape Casting with Addition of Poreformer 48

5. COMPARISON OF DIFFERENT METHODS AND DOWNSELECT 50

6. FILLING CERAMIC SCAFFOLDS WITH THERMAL BATTERY ELECTROLYTE 52
   6.1. Introduction 52
   6.2. Methods 52
      6.2.1. Dipping into melted eutectic salt 52
      6.2.2. Filling with LiCl/KCl aqueous solutions 53
      6.2.3. Gradual temperature increase 54
      6.2.4. Conclusions 55

7. SINGLE CELL TESTING 56

7.1. Test Procedure 56
7.2. Performance of traditional pressed pellet technology 57
7.3. Performance of sintered separator thin film technology 59
7.3.1. Gelled MgO samples 59
7.3.2. Poreformer tape 61
8. CONCLUSIONS 64
9. References 66

FIGURES

Figure 1. Initial Fisher MgO powder before contact with water 15
Figure 2. (top) Particle size distribution of MgO powder used, initially and after ball milling. (bottom) Mass median diameter (of an equivalent spherical particle) after various times on the ball mill. 16
Figure 3. Magnesium oxide hydrolysis during ball milling in water and in 0.1 M HCl 17
Figure 4. The initial modulus of aqueous MgO suspensions (12.5 volume % MgO in a solution of 0.1 M HCl) decreases with time on the ball mill, but continues increasing with time when the sample is allowed to rest after milling 18
Figure 5: Comparison of Small and large strain measurements of 12.5vol% MgO in 0.1MHCl and 0.01% gellan. Large strain measurements were performed at a constant stress of 3Pa at 0.56Hz (initial strain of 800%) and the small strain measurements were performed at a constant strain of 0.01% at 1Hz frequency (initial stress of 0.01Pa). 19
Figure 6. Green sample morphology after A) 0 hrs B) 2 hrs C) 4 hrs D) 6 hrs of drying 20
Figure 7. Low resolution green sample images after A) 0 hrs B) 2 hrs C) 4 hrs D) 6 hrs of drying 21
Figure 8. Porosity of samples created with 12.5% MgO in 0.1 M HCl with various amounts of milling times. 22
Figure 9. Porosity of samples created with varying initial concentrations of MgO in 0.1 M HCl. All samples were milled for 1 hr and dried slowly. 22
Figure 10. Typical sintered microstructure of gelled MgO suspensions 23
Figure 11. Ionic permeability of sintered MgO battery separators 24
Figure 12. Fracture load applied by a 2 mm diameter post of sintered MgO battery separators.. 25
Figure 13. Typical 20X microscope images of emulsions, diluted for easier image processing, and resulting drop size distribution. 27
Figure 14. Cryogenic scanning electron microscopy image of a magnesium oxide Pickering emulsion confirming that the MgO is stabilizing the oil-water interface 29
Figure 15: Concentrations of magnesium oxide (vol % in water phase) and valeric acid (mM in water phase) that produce stable Pickering emulsions containing 70 mL of octane 29
Figure 16: Pickering emulsion tape casts (left) and abstract form (right) 30
Figure 17. SEM image of a sintered (1400 °C) and fractured MgO Pickering emulsion containing 70 vol% octane, 350 mM valeric acid, and mixed at 2000 RPM. 30
Figure 18. Amount (wt%) of brucite in dried green Pickering emulsion samples for varying amphiphile concentration (mM), gellan gum concentration (%), and MgO concentration (vol%)

in the water phase. Error bars represent an estimate based on comparison with TGA measurements of samples without organic material. 32
Figure 19. Shrinkage of samples during sintering at 1400 °C versus the amount of brucite measured in the green state. The line represents the shrinkage expected by a nonporous sample. Error bars represent ± one standard deviation in three measurements per sample. 32
Figure 20a,b: Emulsion drop size as a function of mixing speed and magnesium oxide concentration (vol %) in the water phase. Error bars represent ± one standard deviation of the drop size distribution. For Figure a, the samples were restricted to 10 vol% MgO. For Figure b, the emulsion composition is otherwise the control composition described in the text. 34
Figure 21. Total porosity of samples containing various concentrations of octane after sintering at 1400 °C. . Error bars represent ± one standard deviation of three measurements of porosity for each sample. 35
Figure 22. Sample porosity vs. concentration of magnesium oxide in the water phase for samples containing 350 mM valeric acid, 70% octane, and mixed at 2000 RPM. Error bars represent the pooled uncertainty in the mean based on a Student t test at 95% confidence level. 36
Figure 23. Mean sintered porosity of all samples with a green porosity above 90% when sintered at different temperatures. Error bars represent the pooled uncertainty in the mean based on a Student t test at 95% confidence level. 37
Figure 24. Flake-like structure characteristic of brucite as seen in a sintered Pickering emulsion sample 38
Figure 25: Impedance of Pickering emulsion samples as well as gelled MgO samples not containing octane. An ideal case (solid line) is drawn for samples with nontortuous pore spaces. All circles are Pickering emulsions. Red circles are flake-like, green circles are amorphously shaped (MgO-like), blue circles are odd shaped that fit neither category. Clear circles were not examined with SEM. Black diamonds are gelled MgO samples. 39
Figure 26: Force required on a 2mm diameter post to fracture samples of various porosities. 40
Figure 27. Schematic of replication technique 41
Figure 28. Photo of foam discs used as sacrificial templates to produce foamed ceramics. 42
Figure 29. MgO ceramic discs made with a foam replication technique. 43
Figure 30. Photo (left) and schematic (right) of tape casting system. 44
Figure 31. Laminated substrate formed from stacking and pressing layers of green ceramic tape. 45
Figure 32. Steps to prepare laminates for sintering showing (A-C) them sandwiched between flat plates of MgO and (D) dusted with MgO powder. 46
Figure 33. Sintered tape cast with a punched hole array 47
Figure 34. Images of MgO ceramics made with a foam replication technique. 47
Figure 35. SEM image of a cross section of a 40% PTFE poreformer sample 48
Figure 36. Sample porosity for 10 layer PTFE poreformer samples sintered at various temperatures 48
Figure 37. MacMullin number for 10 layer PTFE poreformer samples sintered at various temperatures 49
Figure 38. Impedance values for all sample types 50
Figure 39. Strength values for all sample types 51
Figure 40. SEM images showing cross sections of a Pickering emulsion sample (left) and a poreformer sample (right) filled with salt using the aqueous solution method 54

Figure 41. Electrolyte salt does not wet Pickering emulsion samples. Salt was melted in a vacuum furnace, cooled, and removed to the atmosphere. 55
Figure 42. Constant current and pulsed current load profile for 1 inch diameter pellets 57
Figure 43. Voltage of single cells composed of 1 inch diameter pressed pellets under a constant current load of 50 mA/cm2 58
Figure 44. Voltage of single cells composed of 1 inch diameter pressed pellets under a pulsed current load 58
Figure 45. Voltage of single cells composed of an anode, cathode, and 1 inch diameter gelled MgO separator, compared to a pressed pellet (E1C) under a constant current load of 50 mA/cm^2 60
Figure 46. Voltage of single cells composed of an anode, cathode, and 1 inch diameter gelled MgO separator, compared to a pressed pellet (E1C) under a pulsed current load..... 61
Figure 47. Voltage of single cells composed of an anode, cathode, and 1 inch diameter gelled MgO separator, compared to a pressed pellet (E1C) under a constant current load of 50 mA/cm^2 62
Figure 48. Voltage of single cells composed of an anode, cathode, and 1 inch diameter poreformer tape separator, compared to a pressed pellet (E1C) under a pulsed current load. 63

TABLES

Table 1. Single Cell Pellet Dimensions 56
Table 2. Gelled MgO separators tested in a constant current single cell battery..... 59
Table 3. Gelled MgO separators tested in a pulsed current single cell battery..... 60
Table 4. Poreformer tape separators tested in a pulsed current single cell battery..... 62
Table 5. Poreformer tape separators tested in a pulsed current single cell battery..... 63

NOMENCLATURE

A	Area
BN	boron nitride
d	drop diameter
EIS	Electrical impedance spectroscopy
G'	Storage modulus, the solid-like contribution to the measured stress response
G''	Loss modulus, the liquid-like contribution to the measured stress response
h	Pellet thickness
H_2O	Water
HCl	Hydrochloric acid
KCl	Potassium chloride
LCl	Lithium chloride
N_m	McMullin number or ratio of the resistivity of the separator to the resistivity of the electrolyte alone
MgO	Magnesium oxide
$Mg(OH)_2$	Brucite
p	probability of obtaining a test statistic at least as extreme as the one that was actually observed, assuming that the null hypothesis is true
PTFE	polytetrafluoroethylene (Teflon®)
R	Resistance
SEM	Scanning electron microscopy
TGA	Thermal gravimetric analysis
v	mixing speed
φ_c	Connected porosity
ρ	Specific resistivity, $\rho = RA / h$

1. INTRODUCTION

Battery separators are placed between the anode and cathode in a battery to prevent shorting of the electrodes while allowing ionic charge transport to complete the circuit. The separators in thermal batteries, the main power supply used in weapon systems, are produced by the labor-intensive pressing of a magnesium oxide-electrolyte powder blend into pellets. Although only comprising ~30% of the volume of a separator pellet, the currently used magnesium oxide (MgO) powder (Merck MagLite S) somehow minimizes the deformation of the pellet during activation (when the electrolyte melts) and prevents leakage of the electrolyte (Guidotti and F. W. Reinhardt, 1996). Regrettably, this particular MgO (MagLite S) powder is no longer produced, so a replacement is necessary. In addition, there is a need to provide more functionality in a limited amount of space, leading to requirements for smaller and lighter batteries. Unfortunately, pressed separator pellets are too brittle if made thin, so battery stack heights are difficult to reduce while maintaining power output, especially for the larger diameter batteries. Furthermore, material movement in thin separator pellets over long discharge times could lead to a short circuit between the anode and cathode and potential thermal runaways (Guidotti et al., 2006). Finally, stack slippage has been observed in some shock tests, possibly because of the lack of strength of the pressed separator pellets. We report novel manufacturing processes for separators that could lead to a much needed replacement for a critical material that is no longer available. Other benefits of these new processes include improved strength, decreased production costs, and shorter battery stacks for the long-life batteries.

Here, we explored the feasibility of manufacturing a strong macroporous ceramic film that can be backfilled with electrolyte to form rigid separators, which is a process that could be done routinely at Sandia to avoid the vagaries of relying on commercial products. Sintered ceramic separators have been tested by Argonne National Laboratories and others (Bandyopadhyay 1982) and offer a promising means to replace MagLite S. However, it is difficult to obtain the high porosity needed in a separator, but low porosity materials yield batteries with high impedance caused by a lower electrolyte loading (Guidotti et al., 2006). On the other hand, rigid, highly porous ceramics filled with electrolyte could allow thinner, stronger, separator layers. Additionally, large sheets of separator material could be made in a batch, and then individual pellets could be punched/cut as needed, streamlining manufacturing processes and eliminating the need to individually press pellets.

The work presented here has other potential applications. For instance, battery separators are also used in commercial lithium ion batteries, and ceramic battery separators are desirable over polymer or fiber based separators due to their chemical resistance and thermal and dimensional stability (Arora and Zhang, 2004). Ceramic separators could allow safe operations of lithium ion batteries at higher temperatures (Song et al., 2011). In addition, porous and permeable ceramic scaffolds are useful to many applications ranging from catalyst supports, filters for molten metal alloys, supports for biomedical tissue growth, capture of solar thermal energy, and high temperature insulation. (Nettleship, 1996; Rice, 1998; Michael Scheffler and Colombo, 2005; Studart et al., 2006)

The challenge is to create highly porous ceramic foams that meet the complex materials and compatibility requirements of a battery system, including wetting properties, dimensional stability, pore size and connectivity, and electrical resistance. Furthermore, it is desired to create such a scaffold from magnesium oxide (MgO), which is chemically compatible with the thermal batteries of interest and has demonstrated favorable wetting properties with the chosen electrolyte. In this application, the separator quality is both dependent on its permeability and its mechanical strength, since it is desired to package the battery under an axial load to ensure all of the components are in electrical contact.

A quality battery separator has high electrical insulating properties to prevent short circuits, yet has high ionic mobility. Ionic resistance is both a function of the separator thickness and ionic transport through the material. Traditionally, the ionic resistance is measured using electrical impedance spectroscopy (EIS) (Barsoukov and Macdonald, 2005; Orazem and Tribollet, 2008). The ratio of the resistivity of the separator to the resistivity of the electrolyte alone is termed the MacMullin number, N_m, which is a material property that takes into account both the tortuosity and the porosity of the material (MacMullin and Muccini, 1956). For perspective, common lithium ion battery separators have MacMullin numbers of 6-12 (Arora and Zhang, 2004).

We explored several methods of producing ceramic foams and tested the resulting materials for strength, the ability to be backfilled by the electrolyte, and MacMullin number. The best candidates were then tested in single cell stacks, each containing one cathode, one anode, and a separator placed between stainless steel current collector plates. Samples were discharged between heated metal platens within a dry and oxygen free glove box, and an Arbin Instruments BT2000 battery tester was used to apply either a constant current or a pulsed current load and monitor the resulting battery voltage.

In the next three sections, three manufacturing processes are detailed. In Section 2, MgO is allowed to gel in water and then sintered. Section 3 describes a similar process in which there is the additional step of adding octane to form a Pickering emulsion to increase the porosity of the final ceramics. Section 4 describes more traditional ceramic processing methods using sacrificial organic materials that decompose during sintering, leaving behind pores. Each section includes discussion of the development efforts, as well as results of strength and ionic mobility measurements. Section 5 summarizes the results from the previous four sections and compares the methods, leading to a down-select of ceramic prototypes to test in a single-cell battery. Section 6 describes several methods tested to backfill the ceramic foams. Section 7 describes the single cell testing done to date. Finally, the last section offers conclusions and recommendations for further work.

2. GELLED MAGNESIUM OXIDE SEPARATORS

2.1. Introduction

We report a method for producing highly porous MgO ceramics with commercially relevant MacMullin numbers (≤12) by tape casting destabilized suspensions of MgO. When magnesium oxide is added to water, a hydrolysis reaction occurs, producing magnesium hydroxide, also known as brucite, $Mg(OH)_2$, and increasing the pH of the suspension ($MgO + 2H_2O \leftrightarrow Mg(OH)_2 + OH^-$). As the suspension nears the brucite isoelectric point of 11, (Pokrovsky and Schott, 2004) the particles destabilize, aggregate, and form a fractal gel. When dried, this gel is a porous, open structure. Sintering strengthens the ceramic scaffold and dehydrates the brucite to MgO. Many processing parameters influence the amount of brucite formation such as pH (Fruhwirth et al., 1985; Merwe et al., 2004; Phillips et al., 1977), drying time, and surface-active additives (Amaral et al., 2011), which in turn affect the porosity and ionic conductivity of the separator. The effects of some of these factors will be reviewed as well.

2.2. Materials and Methods

2.2.1. Sample Preparation

Aqueous dispersions of 2.5 – 17.5 vol% MgO particles (Fisher Scientific) were ball milled with 10 mm zirconium milling media to break up aggregates and disperse the particles. Hydrochloric acid (HCl, 1N, Fluka Analytical) was added (with a few exceptions) to the dispersion before milling to try to maintain a pH between 9 and 10 while milling. The pH of the aqueous solution affects how much brucite is formed and how well the particles disperse. Variable durations of ball milling were explored, ranging from 1 to more than 20 hours. Polymer binder, either 0.01-0.05wt% gellan (CP Kelco), or 0.01 wt% polyvinyl alcohol (PVA) (100,000 g/mol, 87% hydrolyzed, Fisher Scientific), was sometimes added to prevent cracking on drying. The effect of short chain amphiphiles such as valeric acid (99%, Acros Organics) was also studied. The amphiphiles attach to the surface of the magnesium oxide and change the wetting properties of the particles as will be discussed more in the next section on Pickering emulsions. Amphiphile adsorption was also hypothesized to affect the MgO hydrolysis reaction. These species were added after the ball-milling process.

Samples were tape cast by hand on a silicone coated Mylar substrate using a blade coater with gaps of 2, 1, and 0.5 mm or cast into Teflon molds (3 cm diameter, 3-6 mm thick). The samples were either dried quickly at ambient conditions (drying time < 12 hr), or dried more slowly, either covered with a tray or dried in a desiccator over a saturated aqueous potassium chloride solution to control relative humidity at 84% at 25°C (Lide, 1996). Once dry, the samples were removed from the Teflon substrate and sintered in a furnace (Thermolyne 46200) above a light dusting of MgO to aid in reducing shrinkage stress. Organic species burnout, including polymer binder and amphiphiles, and loss of chemically absorbed water was accomplished with a 2 hr hold at 650 °C, and then the samples were ramped to a final sintering temperature of 1400 °C

over 12 hrs, with a 12 hr hold at temperature. Despite significant shrinkage during sintering, final tape cast samples were flat with thicknesses as low as 0.3 mm. Sample thickness was limited by the green sample strength.

The sintered tape was laser cut into pellets with a 400 Watt 1060 nm EDI CO2-Laser; model G-150 (Tucson, AZ). Each sample was placed onto a sheet of 0.010in thick alumina (ADS-96R, from Coorstek, Grand Junction, CO) which acted as a support while the MgO samples were being machined. Each sample was cut with the following laser parameters: 9 ms pulse period, 150-200 μs pulse width (depending on the thickness of the sample), 0.080 in/sec feed rate, and air pressure of 5 psi. The laser beam was focused on the top MgO surface (±0.005 in depending on the sample).

2.2.2. Characterization

The mean particle size after various amounts of milling were determined with a Malvern Mastersizer 3000 laser diffraction particle size analyzer. The amount of brucite that formed during this process (when no gellan or other organics were added) was determined by thermal gravimetric analysis (TGA) using a Netzsch STA 409 PC TGA/DTA DSC under argon that has been filtered for oxygen and water. Slurry rheology was monitored using a TA Instruments AR-G2 rheometer.

Both green and sintered ceramics were imaged with scanning electron microscopy (SEM) using a Zeiss Ultra Plus FESEM and a FEI Quanta 3d FEG. The final density of a sintered sample was measured by estimation of the sample dimensions and weight (Mettler Toledo, XS1003S). The fraction of open pore volume was estimated by an Archimedes test by measuring the fraction of pores that could be filled with water under a vacuum (-0.8 mPa gauge pressure). The strengths of sintered samples were tested with a TA.XTPlus texture analyzer (Texture Technologies) with a 2 mm diameter stainless steel punch.

The ionic conductivity of the ceramic filled with a salt solution was measured using electrochemical impedance spectroscopy (EIS). Samples were filled with an aqueous electrolyte solution (0.85 M KCl conductivity standard, Fisher Scientific) and sandwiched between stainless steel electrodes. A Solartron SI 1287 potentiostat and a Solartron 1255B frequency response analyzer were used to impose an AC voltage (10mV amplitude) of varying frequency (0.01-300,000 Hz) across the separator. The resulting sinusoidal current is measured, and the complex impedance as a function of frequency is inferred. The resistance of the separator is measured at the frequency where the complex impedance is exactly in phase with the imposed AC voltage with no detectable capacitance. Each resistance was measured more than three times and an average reported. The specific resistivity, ρ, of a sample with area A, resistance R, and thickness h is calculated as: $\rho = RA/h$. The MacMullin number N_m is calculated as the ratio between the resistivity of the separator to that of the electrolyte alone, and N_m is always greater than one.

2.3. Results

2.3.1. Effect of Ball Milling and the Hydrolysis of Magnesium Oxide

As purchased, Fisher MgO particles are polydisperse, rod shaped particles (~10-20 μm long) that are composed of a loose packing of cubic MgO crystals (~0.2 μm) (Figure 1). These particles are added to water and ball milled to homogenize the dispersion. Ball milling dispersions of 12.5 vol% MgO in an aqueous solution of 0.1 M HCl for 20 hours decreased the average particle size from a mean of about 10 to 2 μm, determined with a Malvern Mastersizer 3000 laser diffraction particle size analyzer. Less time on the ball mill caused a smaller shift in the size distribution (Figure 2). Ball milling breaks up aggregates and fragments the brittle particle rods. Furthermore, immediately after the particles are in contact with water the MgO hydrolysis reaction begins which can also affect the particle size. Over our three-year project, many different lots of MgO were used for the study of both gels (Section 2) and Pickering emulsions (Section 3). Particle size distributions for material from two lots ordered over two years apart are also shown in Figure 2. For clarity, only subsets of the data acquired after various milling times are shown here. Although slight changes in the particle distribution are evident here, we never saw an effect of changing material lots on the results described in the following sections.

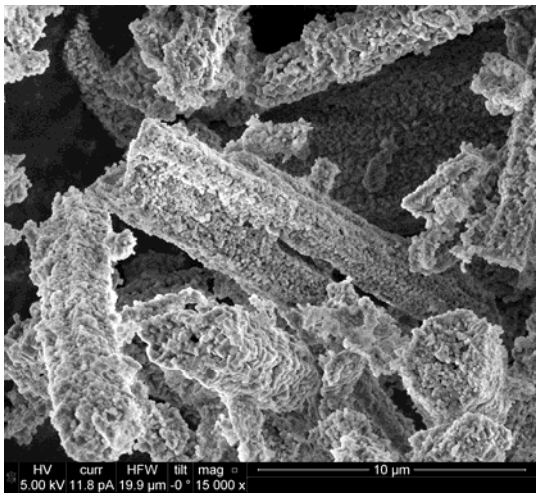

Figure 1. Initial Fisher MgO powder before contact with water

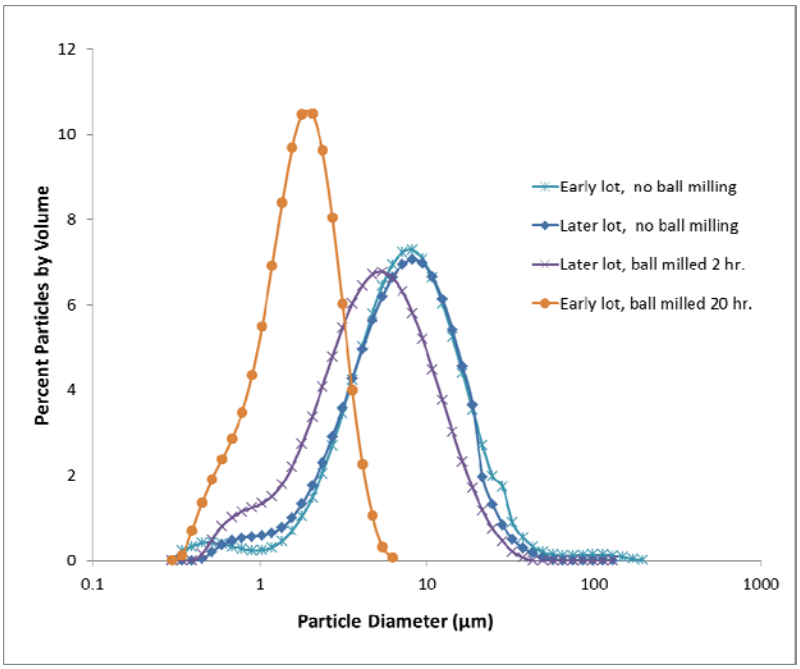

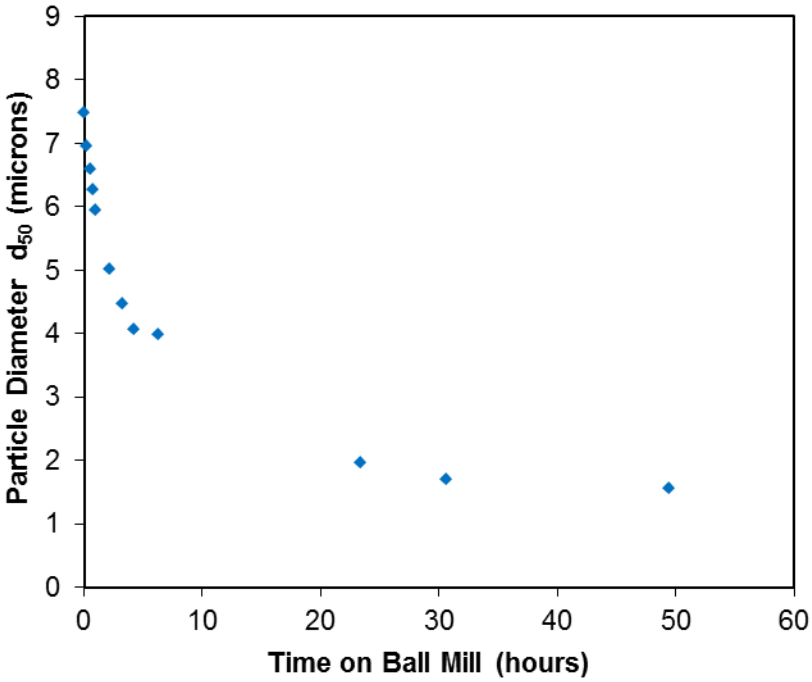

Figure 2. (top) Particle size distribution of MgO powder used, initially and after ball milling. (bottom) Mass median diameter (of an equivalent spherical particle) after various times on the ball mill.

As the MgO is ball milled in water, hydrolysis occurs, turning the MgO to brucite. The hydrolysis reaction is monitored by removing a small amount of the suspension after various amounts of ball milling and rapidly drying the sample at 80 °C in an oven. The amount of

brucite is then measured in a TGA (Figure 3). When 12.5vol% by volume MgO is added to pure water, the brucite concentration in the solid fraction is 30 wt% after 1 hour and 45 wt% after six hours. The reaction is initially rapid and then slows as the pH of the water increases with time. As observed elsewhere, (Fruhwirth et al., 1985; Phillips et al., 1977) the hydrolysis reaction is faster at more acidic pH. When added to acidic solutions, the conversion reaches 50 wt% initially, and after six hours the conversion is at 80 wt%. These results and the purity of the initial MgO were confirmed using X-ray powder diffraction.

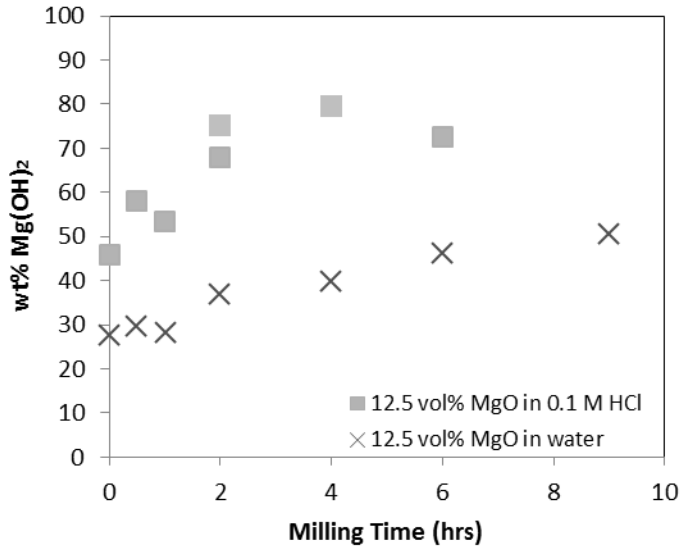

Figure 3. Magnesium oxide hydrolysis during ball milling in water and in 0.1 M HCl

As the pH of the suspension nears its isoelectric point, the brucite will become unstable and aggregate to a gel. These aggregates are fragile and can be broken apart with shear. A suspension of MgO that would turn into a solid sitting quiescently on the bench top will remain a liquid when subjected to strong shear on the ball mill. The hydrolysis and gelling of the MgO occurs whether or not HCl is added to the slurry; however, HCl is added to promote the brucite conversion, leading to faster gelling, which in turn helps prevent particle settling during drying as will be discussed in the following paragraphs. These transitions can be studied by examining the rheology. Using linear oscillatory rheology at very small strains, the gelling process can be measured without disruption to the developing internal gel structure. In order to preserve the structure, very low strains were required. Figure 4 shows the rheology of the 12.5vol% MgO suspensions in 0.1M HCl as a function of residence time on the ball mill with an applied strain of 0.01% (a strain amplitude of <1 micron). For each of these suspensions, the measured modulus increases rapidly with time, and within an hour or two of removal from the ball mill, the suspension has gelled into a solid. As the suspensions are ball milled longer, large aggregates of MgO are broken up into smaller particles resulting is a softer aggregated network. In all cases however, the response of the suspension is primarily in phase (G') with the applied sinusoidal strain oscillation indicating the elastic character of these suspensions ($G'>G''$).

By contrast, if a large strain is applied to the suspensions, the response of the MgO suspensions is fundamentally different as observed in Figure 5. In this case, the applied deformation was specified as a constant stress of 3 Pa which resulted in initial strains of 800%. In this large strain

regime, instead of a primarily elastic response caused by the early formation of a network of aggregated MgO particles, the response of the suspension is out of phase to the applied strain indicating a viscous response (*G"*>*G'*) due to dissipation as particle are pushed past each other. The increase in the modulus occurs much more gradually as the growing increase in particle attraction competes with the shear forces pulling particles apart. The particle attraction eventually wins out and the final gel transition is much more dramatic but occurs at a similar time to that observed in the small strain experiments. This is consistent with progression of the hydrolysis chemical reaction driving the gelation as opposed to kinetic or diffusion limited processes. In these large strain experiments, the initial modulus increases with ball-mill time as the overall viscous dissipation in a suspension is increased as aggregates are broken down into smaller particles during the ball mill.

The modulus of the final gelled suspension is only a weak function of time on the ball mill with longer ball-mill times perhaps resulting is weaker suspensions. This trend may be caused by the effects of particle settling during the rheology measurement. Suspensions that were only ball milled for 30 min showed significant settling with a clear layer of 5-10% water at the top of the suspension. This resulted in a higher MgO concentration in the final gelled region. Only slight settling was observed in the 1-hour ball-milled suspensions (<3%) and no settling was observed for longer ball-mill times.

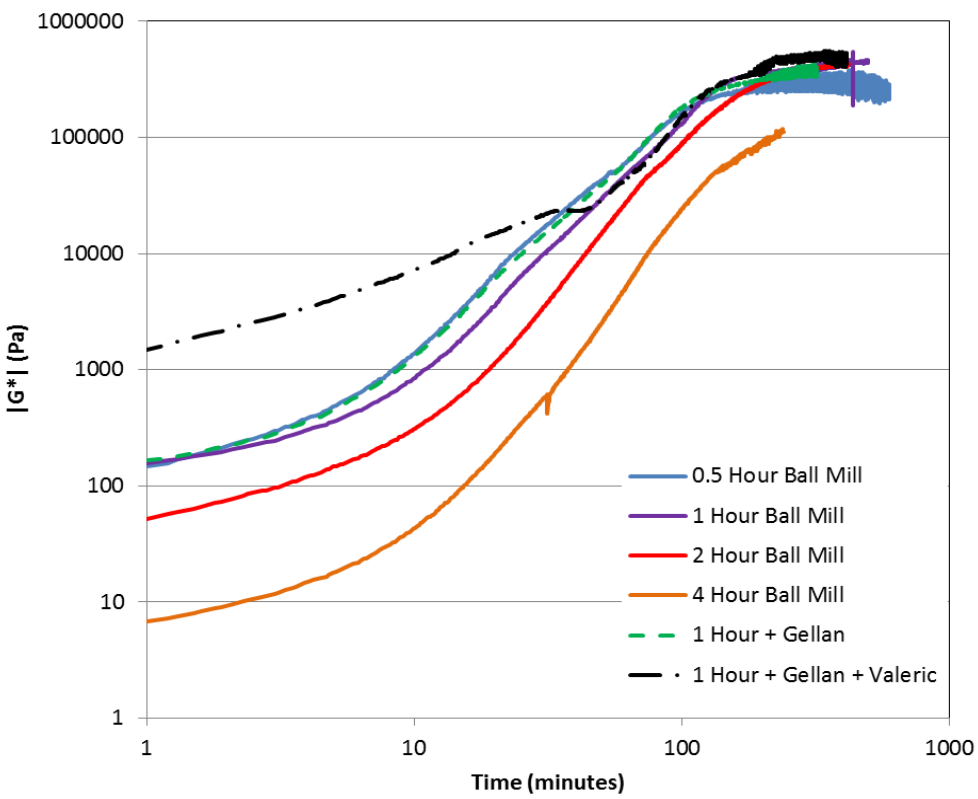

Figure 4. The initial modulus of aqueous MgO suspensions (12.5 volume % MgO in a solution of 0.1 M HCl) decreases with time on the ball mill, but continues increasing with time when the sample is allowed to rest after milling

The impact of other emulsion additives is demonstrated in Figure 4. Gellan is used to improve green sample robustness. This polysaccharide is not expected to interact with the particles and this is confirmed by the rheology. The addition of 0.01wt% gellan only moderately increases the modulus of the suspension, likely the result of an increase in the aqueous phase viscosity. Valeric acid is expected to absorb onto the MgO particles and modify their surface chemistry to enable a stable Pickering emulsion as will be discussed in the next section. That strong interaction with the suspension particles is apparent in the large increase in the measured modulus, indicating that the particle attractions and resulting aggregation are stronger in the presence of valeric acid. It has been speculated that excess valeric acid may increase the viscosity of the suspension by coagulating the magnesium oxide, either by bridging particles or by increasing their hydrophobicity so that the particles aggregate (Akartuna et al., 2008b). While the rheology clearly shows increased aggregation, it is not sensitive to the degree of hydrophobicity required to make a stable emulsion.

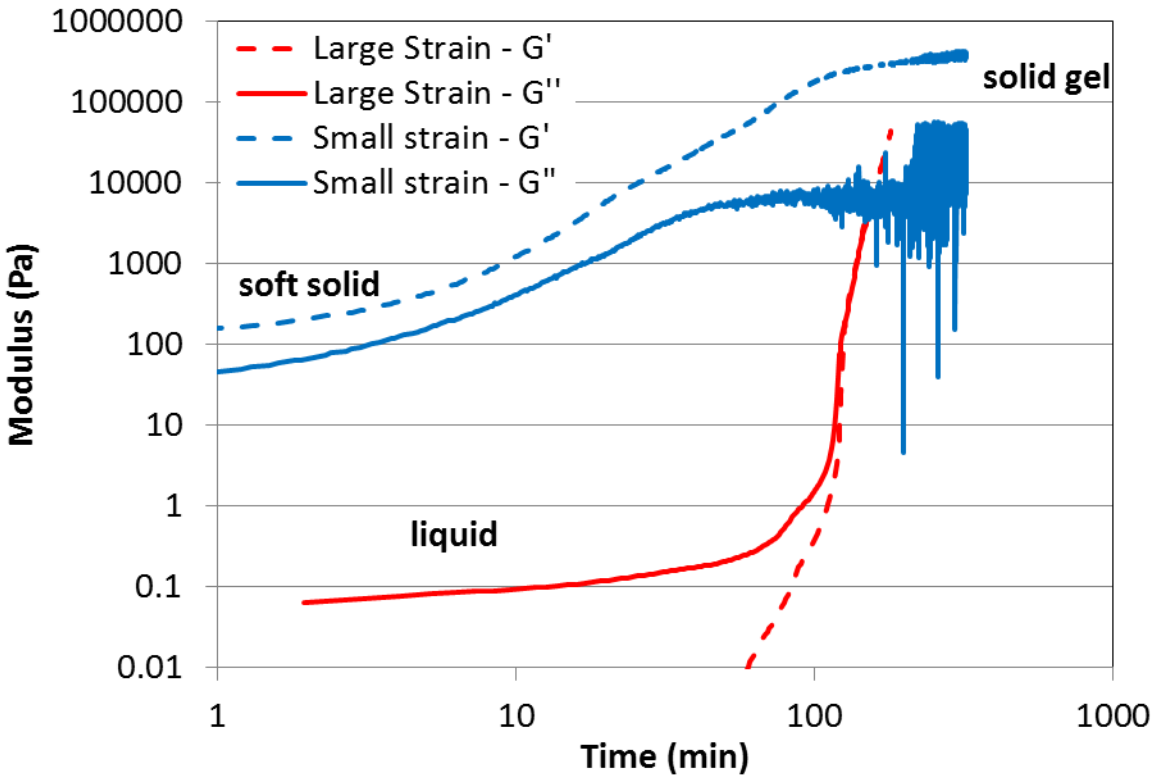

Figure 5: Comparison of Small and large strain measurements of 12.5vol% MgO in 0.1MHCl and 0.01% gellan. Large strain measurements were performed at a constant stress of 3 Pa at 0.56 Hz (initial strain of 800%) and the small strain measurements were performed at a constant strain of 0.01% at 1 Hz frequency (initial stress of 0.01 Pa).

Finally, microstructure changes in the drying samples were observed using scanning electron microscopy. A 12.5 vol% MgO suspension in 0.1 M HCl was ball milled for 1 hour, coated into molds and dried slowly in a confined environment. Every two hours, the remaining liquid in a sample was removed quickly in an oven at 80 °C to stop the hydrolysis reaction.

Figure 6 shows high resolution images of how the individual particle morphology of the unsintered samples starts as a cubic shape, characteristic of MgO. After about four hours of drying, the characteristic brucite flake-like structure (Kumari et al., 2009) is dominant in the sample, as growth of (111) crystal planes are highly favored over others (Mejias et al., 1999). Low resolution images (Figure 7) show that as more brucite forms in the quiescent sample the particles decrease in size, as observed previously in the particle size analysis.

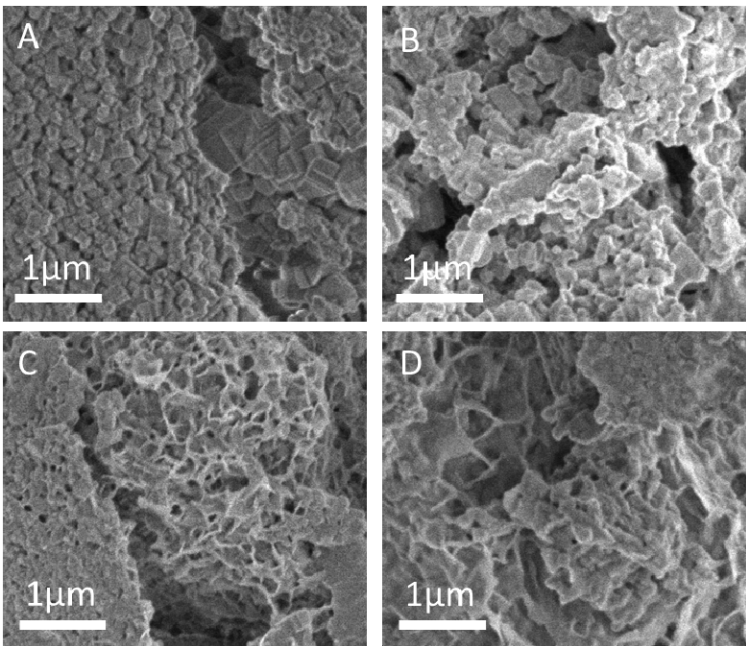

Figure 6. Green sample morphology after A) 0 hrs B) 2 hrs C) 4 hrs D) 6 hrs of drying

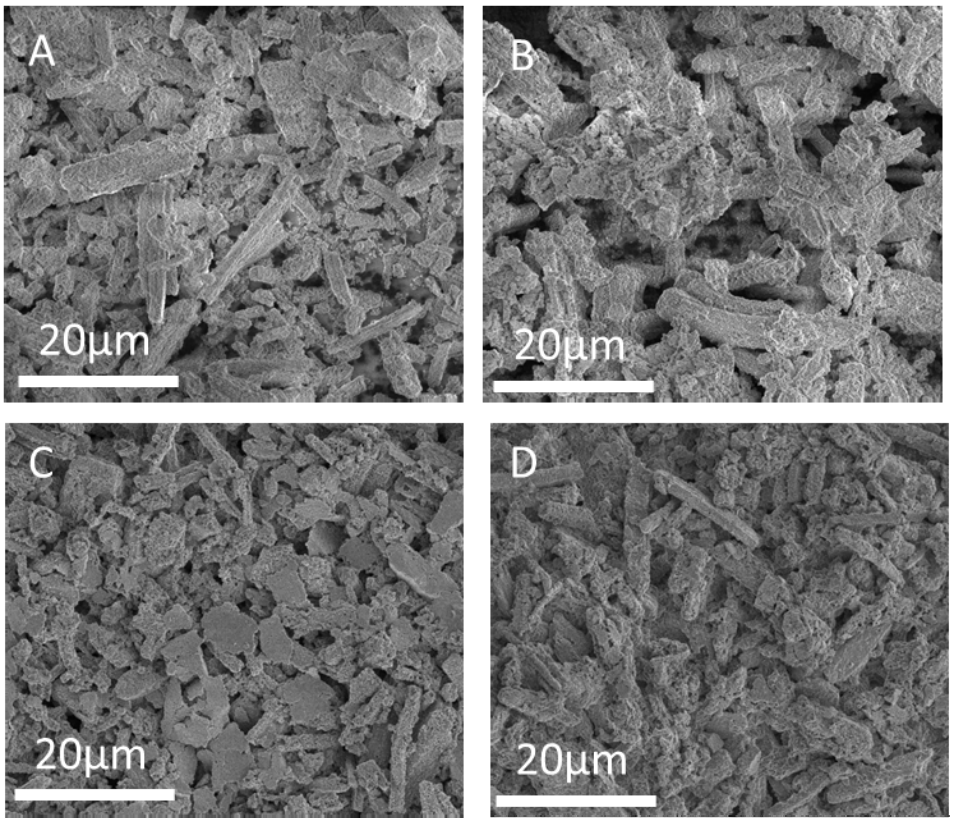

Figure 7. Low resolution green sample images after A) 0 hrs B) 2 hrs C) 4 hrs D) 6 hrs of drying

2.3.2. Sample Porosity

Processing parameters such as formulation and drying time affect the final sintered porosity of the separators. Figure 8 displays the porosity of both green and sintered samples made from a 12.5 vol% MgO dispersion with 0.1 M HCl for various milling times. Samples with long milling times produced more brucite, creating a space-filling gel, whereas samples with low milling times were observed to partially settle to the bottom of the mold before the sample dried, creating a mildly less porous green sample. This effect is apparent in a mild increase in green porosity with milling time. Although small, this increase is statistically significant based on a linear regression with the free statistical package "R" (www.r-project.org).

As the samples are sintered, the brucite dehydrates to magnesium oxide. Brucite has a density (2.39 g/cm^3) that is less than that of magnesium oxide (3.58 g/cm^3), so the samples shrink upon sintering to a degree depending on the amount of brucite that formed during the sample preparation. This can be seen in Figure 8, where the amount of porosity in the sintered samples is much less for higher mill times. Also, samples with high brucite concentrations are more likely to crack and curl upon sintering. Consequently, some brucite is desired on the particle surfaces to destabilize the suspension and create a space-filling particle gel. However, extensive hydrolysis promotes excessive shrinkage and curling on sintering and is undesirable.

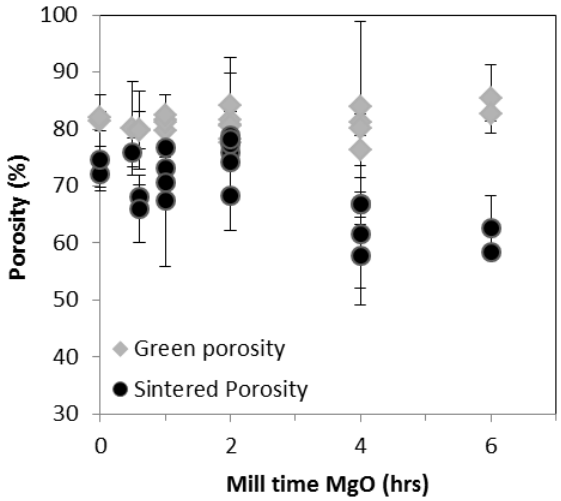

Figure 8. Porosity of samples created with 12.5% MgO in 0.1 M HCl with various amounts of milling times.

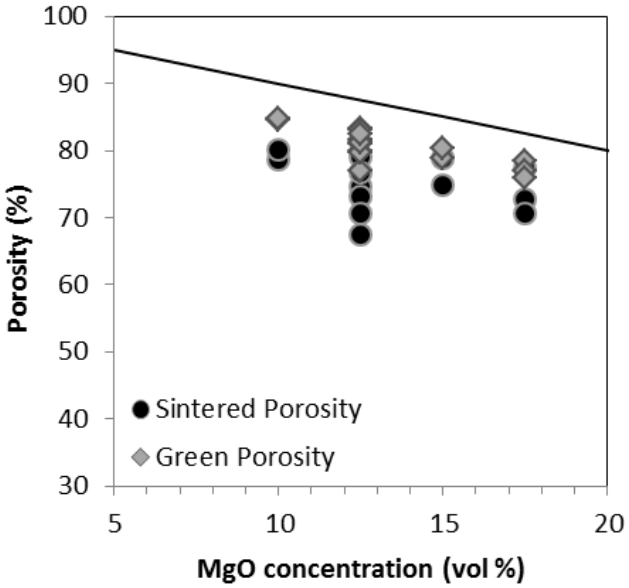

Figure 9. Porosity of samples created with varying initial concentrations of MgO in 0.1 M HCl. All samples were milled for 1 hr and dried slowly.

The concentration of the initial MgO suspension was also varied as shown in Figure 9. In this case, all samples were milled for one hour. The pore space between particles in the green samples was measured to be only 5% less than in the initial MgO dispersion (solid line, Figure 9). This demonstrates that the gelled particle network spanned the entire mold and did not settle or shrink upon drying. It is expected that the hydrolysis reaction would occur to a greater level of conversion in more dilute samples. Samples containing 5 vol% MgO shrank to 75% of their green height, whereas samples containing 17.5 vol% MgO shrank to 85% of their green height upon sintering.

The effects of binder concentration and short chain amphiphiles were also studied. Polymer binders in the concentrations studied were found to increase the robustness of the green samples without noticeably affecting the final, sintered porosity. Addition of valeric acid (at a concentration of 273 mM) also had no significant effect on the final porosity.

The final microstructure of the sintered gelled MgO samples is shown in Figure 10. The rod-like shape of the original Fisher MgO persists, and the particles are randomly oriented, giving the separator an open microstructure. Smaller, irregularly shaped collections of magnesium oxide formed during ball milling or from the hydrolysis reaction fill some of the pore space but also act to cement the rods together.

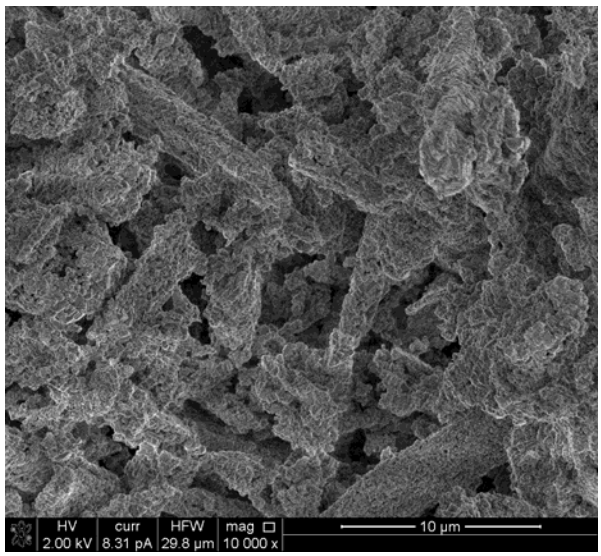

Figure 10. Typical sintered microstructure of gelled MgO suspensions

2.3.3. Separator Quality

Separators were tested for both ionic permeability and fracture strength to determine their suitability for battery applications.

Ionic permeability is affected by both the total connected porosity and the tortuosity of the pore space. The connected porosity determines the volume or cross section available for transport, and the tortuosity influences both the path length and the number of dead ends in the material (Dullien, 1975). Archie's law (Archie, 1942) is a semi-empirical relation between the MacMullin number and the connected porosity, ϕ_c, of unconsolidated porous materials:

$$N_m = a\phi_c^{-m} \quad \textbf{(1)}$$

where a is a parameter and m is the cementation exponent. In a perfect material without tortuosity N_m would be inversely proportional to the connected porosity, or m would be 1 (Balberg, 1986; Dullien, 1975). In common materials, $1.3 < m < 2.5$.

The ionic permeability of sintered separators is measured using electrical impedance spectroscopy and is displayed in Figure 11 with respect to the connected porosity of the samples. The measured MacMullin numbers of the samples suggest that these materials are permeable enough for battery separator applications. The high cementation exponent of 2.12 indicates that the pore space is very tortuous, with not all of the connected porosity contributing to the connected paths between electrodes. Small improvements in the connected porosity correspond to a great benefit in permeability.

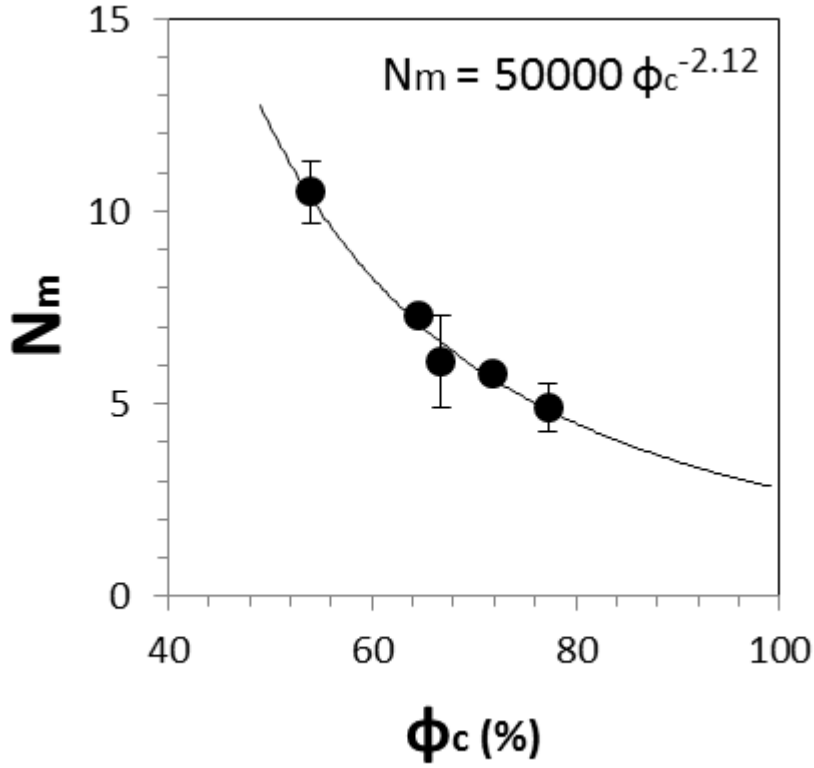

Figure 11. Ionic permeability of sintered MgO battery separators

As the total sintered porosity increases, the compressive strength of the sample decreases. Figure 12 shows the maximum load on a 2 mm diameter post that will not fracture the material. The substantially decreasing loss of strength with porosity is characteristic of many other porous materials (Rice, 1998). A 2 kg load on a 2 mm diameter post corresponds to approximately 900 psi, which is above most closing forces that are used on traditional thermal batteries. Therefore, it is unlikely that the sintered MgO network structure will collapse during battery activation as the pressed pellet separators are known to do. Furthermore, the addition of electrolyte salt to the magnesium oxide pore space will further strengthen the gelled samples at room temperature.

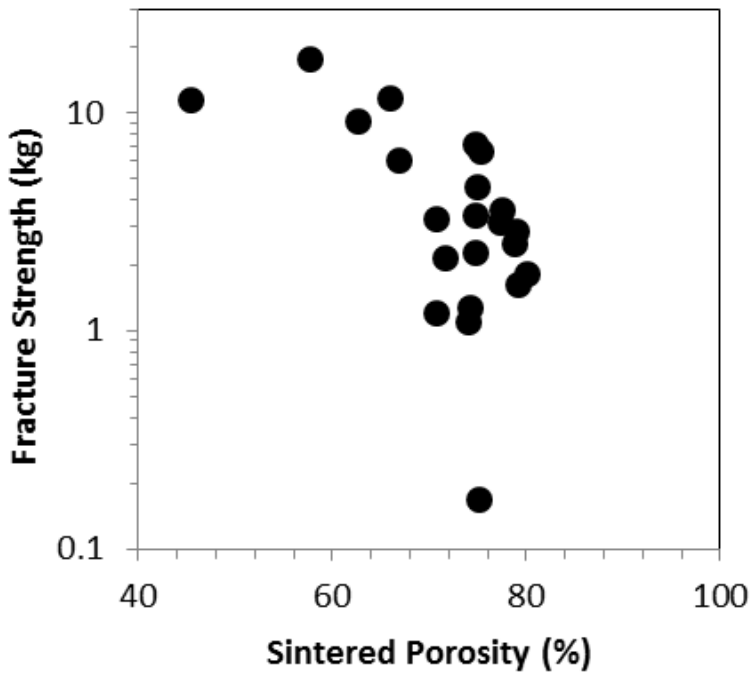

Figure 12. Fracture load applied by a 2 mm diameter post of sintered MgO battery separators

2.4. Conclusions

Separators made by gelling magnesium oxide dispersions were designed to be highly porous structures with properties that were tunable based on processing conditions. For example, ball-milling time, initial pH, and MgO concentration in the dispersion were all factors in creating the desired microstructure. Other additives such as polymer binder improved the initial green strength of the sample, but did not influence the final microstructure. The sample production process is scalable; small tape casts up to 2.5 inches wide were made and sintered successfully, and larger tape casts are presumed to be possible. The final, sintered structure has abundant compressive strength to be built into a thermal battery and promises to have sufficient ionic permeability to compete with existing technology.

3. PICKERING EMULSION MAGNESIUM OXIDE SEPARATORS

3.1. Introduction

Recently, researchers (Akartuna et al., 2009; I. Akartuna, 2009; Imhof and Pine, 1997; Neirinck et al., 2009) have shown that particle-stabilized oil-water emulsions, termed Pickering emulsions (Pickering, 1907), can be dried, leaving only the particles behind in a highly porous but stable foam-like structure. Pickering emulsion properties such as drop size and porosity are adaptable by varying processing conditions. For example, mixing speed (Gurevitch and Silverstein, 2010; Sturzenegger et al., 2012), particle concentration (Arditty et al., 2003; Binks and Whitby, 2004; Sturzenegger et al., 2012), particle wettability (Akartuna et al., 2008b; Bachinger and Kickelbick, 2010; Chuanuwatanakul et al., 2011; Haase et al., 2011), particle aspect ratio (Vandebril et al., 2010), particle roughness (San-Miguel and Behrens, 2012), and particle size (Binks and Lumsdon, 2001) have all been studied. Such wet emulsions can be shaped, extruded into forms or coated into sheets because of their measurable yield stress (Akartuna et al., 2009; Chen et al., 2012). Once dried, the resulting highly porous green ceramics can be sintered, creating a ceramic foam with open cell microstructure and compressive strengths up to 13 MPa and porosities above 70 vol% (Akartuna et al., 2008a).

Particles must equally wet both liquid phases of the emulsion to be stable at the oil-water interface (Finkle et al., 1923). Akartuna et al. (Akartuna et al., 2008b) and others (Brandriss and Margel, 1993; Gonzenbach et al., 2006) achieve this wetting behavior for several types of metal oxide powders by modifying the surfaces with short amphiphilic molecules. However, magnesium oxide has not largely been explored as a Pickering emulsion stabilizer beyond initial studies of hydrogeologic interest (Roy-Perreault et al., 2005). This is because processing MgO in water is challenging due to its propensity to hydrate to brucite as discussed in the previous section. Brucite has a different density, wettability, and crystal habit compared to magnesium oxide.

At the beginning of this project, it was unclear whether amphiphile-modified MgO Pickering emulsions could be used to template ceramic foams. If foams could be created, the effect of MgO hydrolysis on the final, sintered structure would be an important factor to consider as compared to other ceramic Pickering emulsions where no hydrolysis occurs. We also investigated other processing conditions that can affect the Pickering emulsion microstructure. Finally, the resulting porous structures were tested for their suitability for battery applications.

3.2. Methods

3.2.1. Pickering Emulsion Synthesis

Aqueous dispersions of 2.5 – 15 vol% MgO particles (Fisher Scientific) were prepared as previously described in Section 2. Here, HCl was added to create surface groups on the MgO particles that would allow an amphiphile to bind to that surface. After milling, an amphiphile was added at concentrations ranging from 150-500 mM, and the aqueous dispersion was stirred

for 3 minutes. Amphiphiles that help stabilize the emulsions include propionic acid (99%, Sigma Aldrich), butyric acid (99%, Sigma Aldrich), valeric acid (99%, Acros Organics), and hexanoic acid (99%, Sigma Aldrich), although here we focus on results using valeric acid.

Up to 70 vol% n-octane (>99%, Sigma Aldrich) was added slowly to the aqueous MgO dispersion as the liquids were mixed at 200-500 revolutions per minute (RPM) using a Cowles mixer (Dispermat, VMA-Getzmann GMBH). Emulsification was accomplished by vigorously mixing at speeds ranging from 1,000 – 7,000 RPM for two minutes after the addition of the oil. Polymer binder, either 0-0.3 wt% polyvinyl alcohol (PVA) (100,000 g/mol, 87% hydrolyzed, Fisher Scientific) or 0.01- 0.03 wt% gellan gum (CP Kelco), was added to prevent cracking on drying. Gellan has the advantage that it is not surface active and, therefore, should not interfere with the oil-water surface tension or the surface treatment of the MgO with the amphiphile (Park et al., 2008; Paunov, 2003).

Emulsions were tape cast by hand on a silicone coated Mylar substrate or cast into polytetrafluoroethylene (PTFE) molds (3 cm diameter, 3-6 mm thick). The samples were either dried quickly at ambient conditions (drying time < 12 hr), dried more slowly covered (drying time > 48 hours), or dried very slowly in a desiccator over a saturated aqueous KCl solution to control relative humidity at 84% at 25°C (drying time > 72 hours). Once dry, the samples were sintered in a furnace (Thermolyne 46200). Polymer burnout was accomplished with a 2 hr hold at 650°C, and then the samples were ramped to final sintering temperatures ranging from 1250°C to 1675°C over 12 hrs, with a 12 hr hold at temperature. Tape cast samples were laser cut into pellets after sintering as described in Section 2.2.1.

3.2.2. Characterization

Droplet size distributions of wet Pickering emulsions were estimated by viewing diluted emulsions using an inverted optical microscope (Nikon Eclipse TE2000-5) in transmission mode. The droplets were very robust and we observed no effect on the droplet size with the amount of dilution. Images were captured using a camera (Phantom Miro-4M, Vision Research) and analyzed using Image Pro Plus 7.0 software (MediaCybernetics, Inc.). Typically 500 to 1000 drops were analyzed per sample. Typical images are shown in Figure 13.

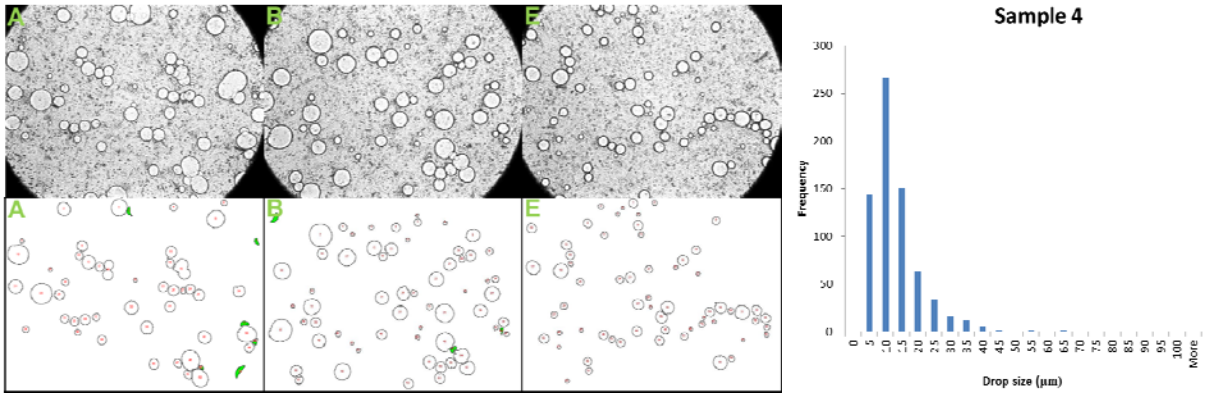

Figure 13. Typical 20X microscope images of emulsions, diluted for easier image processing, and resulting drop size distribution.

Both green and sintered ceramics were imaged with SEM using a Zeiss Ultra Plus FESEM and a FEI Quanta 3d FEG. Cryogenic SEM was performed on a Hitachi 4700 SEM at the University of Minnesota Characterization Facility. Here, the wet emulsion was coated onto a silicon chip and frozen in liquid ethane before it was fractured and coated with platinum in an Emitech K-1250 cryo-preparation chamber. The sample was then imaged at -160 °C.

Since binder and other organics interfered with TGA estimations of the brucite concentrations in dried, green, Pickering emulsion samples, the brucite concentration is measured instead by fitting X-ray powder diffraction scans (Bruker D8 X-ray diffractometer) using GSAS-II Rietveld refinement software, distributed by Argonne National Laboratory. Brucite concentrations measured with X-ray powder diffraction corresponded well with TGA measurements for samples not containing organics, and the maximum difference between the values of concentration given by the two methods for the same sample was used as a conservative estimate of the error in the X-ray powder diffraction fit when reporting the data.

The final density of a sintered sample was measured by estimation of the sample dimensions and weight (Mettler Toledo, XS1003S). The fraction of open pore volume was estimated by an Archimedes test by measuring the fraction of pores that could be filled with water under a vacuum (0.07 MPa). The strengths of sintered samples were tested with a TA.XTPlus texture analyzer (Texture Technologies) with a 2 mm diameter stainless steel cylindrical punch. EIS was used as a measure of the permeability of the sintered separators as described previously in section 2.2.2

3.3. Results

3.3.1. Creation of Magnesium Oxide Pickering Emulsions

Magnesium oxide was found to stabilize an octane-water emulsion containing no additional surface modifiers or binders up to 45 vol% octane; however, a greater amount of octane could be incorporated with the addition of carboxylic acid derived amphiphiles. Successful Pickering emulsions containing approximately 70 vol% octane were produced using various concentrations of valeric, propionic, and butylmalonic acids. In all cases, the emulsions were stable, without visual evidence of droplet settling, for weeks.

Cryogenic scanning electron microscopy images of a MgO Pickering emulsion stabilized with valeric acid are shown in Figure 14. During the sample preparation, the vitrified emulsion was fractured and the octane that filled the droplet fell away. Water is the continuous fluid, whereas octane forms the droplets. Flake-like particles can be seen lining the oil-water interface, confirming that a Pickering emulsion was successfully created. Particle aggregates can also be seen dispersed in the continuous water phase. These unabsorbed aggregates increase the viscosity of the aqueous phase as well as likely sterically inhibit coalescence of the octane droplets (Aveyard et al., 2003).

A stability window for successful Pickering emulsions is detailed in Figure 15 showing the concentrations of MgO and amphiphile where the emulsion was able to contain 70 mL of octane (70% of the emulsion volume) without separation. This plot is limited to a subset of the

Pickering emulsion recipes containing only emulsions that were mixed at 2000 RPM with valeric acid as the amphiphile. Within the range of gellan concentrations tested, we saw little influence of the amount on the ability to create a stable emulsion, therefore the emulsions represented in Figure 15 contain various gellan concentrations unspecified from 0-0.05 wt%. It is found that high octane concentration Pickering emulsions are not possible without valeric acid to decrease the hydrophilicity of the particle surfaces. Pickering emulsions with MgO concentrations greater than 15 vol% are not stable, perhaps because MgO increases the viscosity of the water phase until the octane cannot be emulsified during the mixing step. A third boundary exists at increasing valeric acid and decreasing magnesium oxide concentrations. Again, the increase in viscosity caused by the addition of excess valeric acid (Figure 4) may be the dominant factor in this limit. Alternately, if the MgO particles are made too hydrophobic, they may no longer stabilize the oil water interfaces in the emulsion.

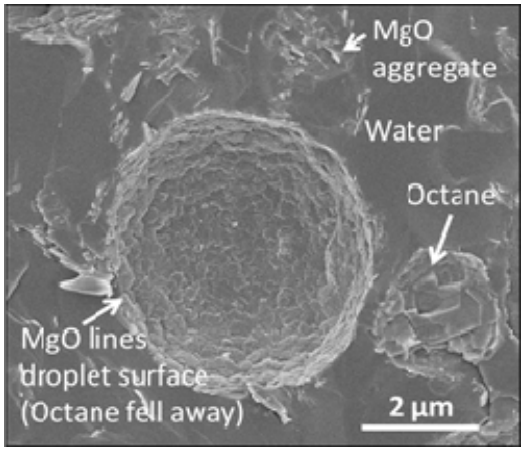

Figure 14. Cryogenic scanning electron microscopy image of a magnesium oxide Pickering emulsion confirming that the MgO is stabilizing the oil-water interface

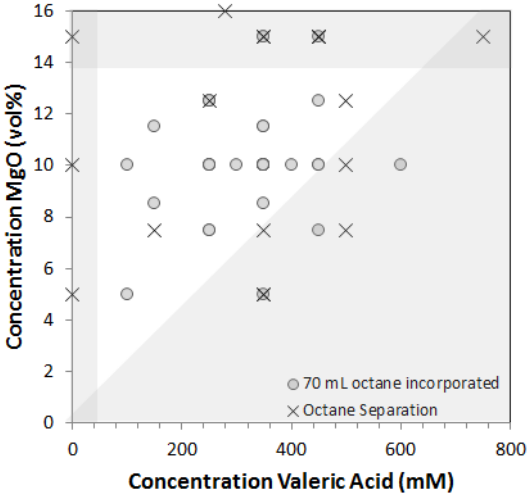

Figure 15: Concentrations of magnesium oxide (vol % in water phase) and valeric acid (mM in water phase) that produce stable Pickering emulsions containing 70 mL of octane

Once formed, the Pickering emulsions are easily molded or cast into shapes, as demonstrated in Figure 16. The emulsions clearly had a yield stress and would keep their shape and mound on a spoon. Unfortunately measurement of the emulsion yield stress was problematic because free

octane caused slip on the measurement fixtures. Yield stresses up to 70 Pa were measured, though the true yield stress may be higher due to the influence of slip. Smooth coatings ranging in thickness from 1 mm to 10 mm were created. Most samples for this study were coated into cylindrical molds, dried, and sintered.

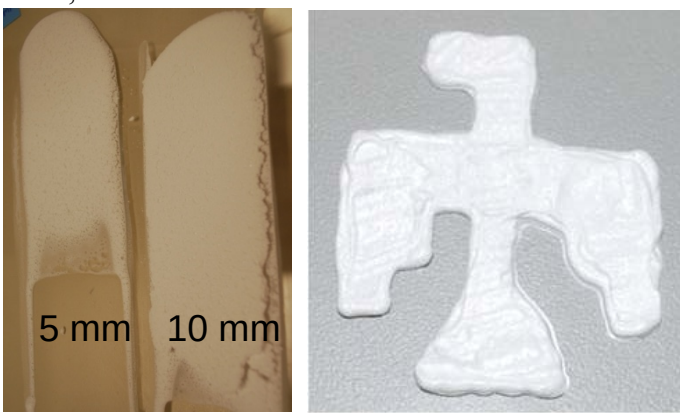

Figure 16: Pickering emulsion tape casts (left) and abstract form (right)

The character of the emulsion visualized with cryogenic scanning electron microscopy is reflected in the final, sintered microstructure. A scanning electron microscopy image of an emulsion-based ceramic that was sintered at 1400 °C is shown in Figure 17. A layer of MgO particles covers the surface of what were once droplet surfaces. Some MgO, which was probably suspended in the water phase, is visible between the droplets, giving the final structure added strength. The sample also appears highly permeable, with large pores created by the droplets and also small pores between incompletely sintered MgO particles.

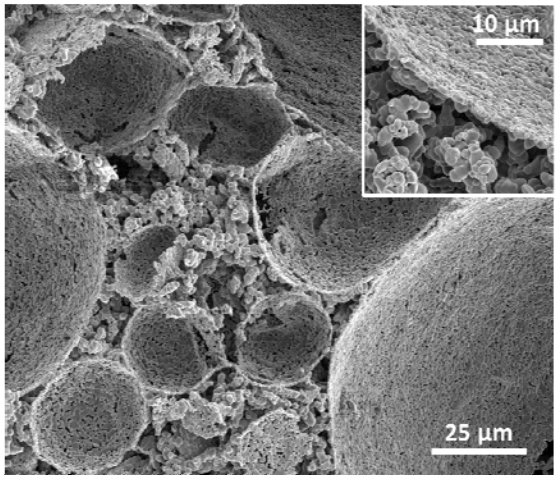

Figure 17. SEM image of a sintered (1400 °C) and fractured MgO Pickering emulsion containing 70 vol% octane, 350 mM valeric acid, and mixed at 2000 RPM.

3.3.2. Effects of Brucite Conversion

Researchers have shown that variables such as emulsion composition (Arditty et al., 2003; Binks and Whitby, 2004; Sturzenegger et al., 2012), mixing speed (Gurevitch and Silverstein, 2010; Sturzenegger et al., 2012), and particle size (Binks and Lumsdon, 2001) have impacts on the Pickering emulsion properties such as porosity and microstructure. When magnesium oxide is used to stabilize the emulsion, processing variables additionally influence the amount of brucite that is created during the sample preparation. Although brucite converts back to magnesium oxide during sintering, brucite has a density (2.39 g/cm^3) that is less than that of magnesium oxide (3.58 g/cm^3), so the samples shrink upon sintering to a degree depending on the amount of brucite conversion that occurred during the sample preparation. Furthermore, brucite exhibits a flake-like crystal morphology which in some cases remains after the sintering process. These properties can affect the final emulsion-based ceramic quality, including the permeability and strength.

A control sample recipe was chosen that contained an aqueous phase containing 10 vol% magnesium oxide, 350 mM valeric acid, and 0.01% gellan gum. The control was then mixed with 70 vol% octane at 2000 RPM and was dried covered with a tray. The amphiphile, gellan, and MgO concentrations were all varied from this control, and the resulting brucite concentration found in the green sample was measured using X-ray powder diffraction (Figure 18). Brucite conversion decreased with MgO concentration. This is because the magnesium oxide hydration reaction causes the pH of the dispersion to increase until the reaction kinetics slow or stop (Fruhwirth et al., 1985). When the MgO concentration in the solution is low, a greater fraction of the ceramic is hydrated before the reaction is slowed. As the gellan concentration is increased, the amount of brucite is first increased, perhaps because the gellan retards the drying of the samples, increasing the contact time of MgO with the water. As the gellan is increased further, the brucite conversion decreases, although we do not know why. Finally, the amphiphile concentration does not have a large effect on the hydrolysis of the magnesium oxide. A trend is observed in which large concentrations of amphiphile slightly decrease the amount of observed brucite, possibly because the attachment of the amphiphile to the magnesium oxide may slow the hydrolysis rate as observed for other surface active organics (Amaral et al., 2011). However, this trend is within our estimated uncertainty limits. The effect may be mitigated by the increase in pH caused by the addition of the acidic amphiphiles.

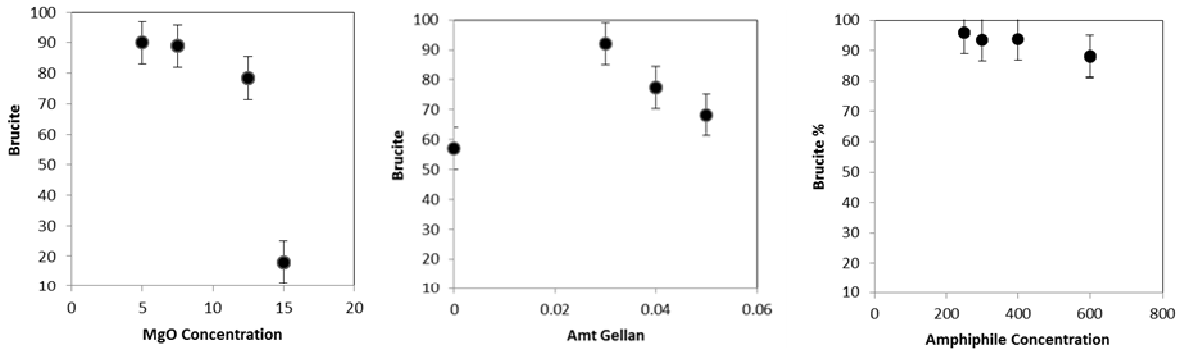

Figure 18. Amount (wt%) of brucite in dried green Pickering emulsion samples for varying amphiphile concentration (mM), gellan gum concentration (%), and MgO concentration (vol%) in the water phase. Error bars represent an estimate based on comparison with TGA measurements of samples without organic material.

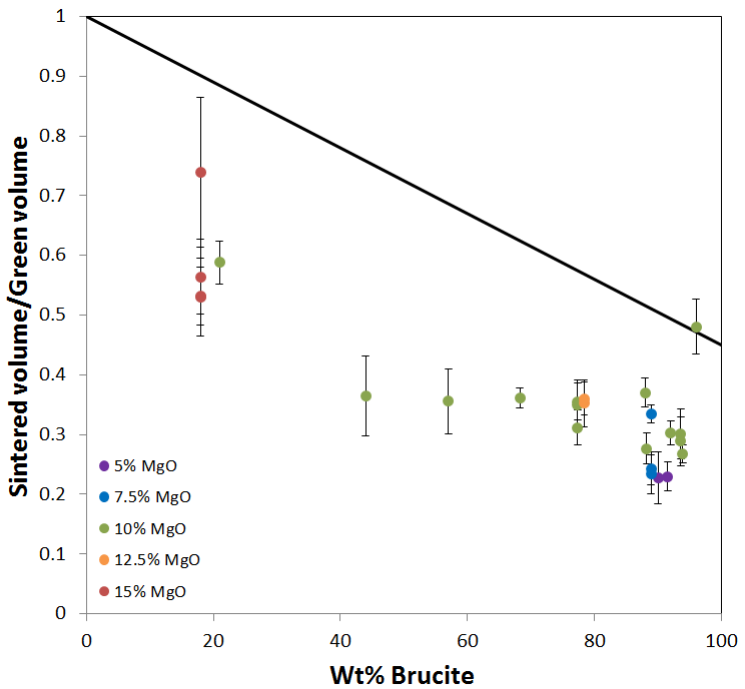

Figure 19. Shrinkage of samples during sintering at 1400 °C versus the amount of brucite measured in the green state. The line represents the shrinkage expected by a nonporous sample. Error bars represent ± one standard deviation in three measurements per sample.

As discussed in Section 2, the MgO hydrolysis is also significantly affected by the length of time the MgO was initially milled. It is found that the brucite conversion begins quickly after addition of the MgO to the acidic dispersion. Within one hour, the conversion reaches 50 wt%, and after six hours the conversion is at 80 wt%. The hydrolysis reaction is slower at more basic pH (Fruhwirth et al., 1985; Phillips et al., 1977). In cases where no hydrochloric acid is added to the initial ball-milled solution, the brucite concentration is 30 wt% after 1 hour and 45 wt% after

six hours. As with the gelled samples discussed in Section 2, some brucite is desirable to increase the viscosity and stabilize the emulsions during processing.

In high humidity environments, the samples dried slowly and brucite conversion was presumed to be higher. In lower humidity environments, the samples dried more quickly, yet these samples were more prone to cracking during the drying step.

The brucite conversion was found to correlate with the sample volumetric shrinkage during the sintering, as expected due to the density difference between the two materials. Figure 19 compares the amount of shrinkage exhibited during sintering at 1400 °C by green samples with a range of brucite concentrations. As the samples are sintered, the brucite is dried to magnesium oxide. The solid line represents the amount of shrinkage expected by a nonporous monolith, due to only the change in density between these two materials. The observed shrinkage of the Pickering emulsions is even greater due to the sintering and densification of the ceramic particle grains. To prevent cracking and to maximize the porosity of the final material, less shrinkage is desired. Figure 19 also reiterates the information in Figure 18, that lower amounts of MgO in general give higher percentages of brucite.

3.3.3. Effects of Material and Processing Variables on Sample Porosity

Material and processing variables studied included amount of MgO powder, type and amount of amphiphile, type and amount of binder, amount of octane, length of time ball milling, and speed of mixing in the octane. It is intuitive that sample composition, especially the concentration of MgO and the amount of brucite developed will affect shrinkage and, therefore, porosity. However, many of the variables interact. For example, if the viscosity resulting from the composition and processing protocol is too low a stable emulsion cannot be formed; however, the viscosity also cannot be too high, either. The amount of valeric acid needed depends on the amount of MgO surface area, which depends on the original amount and the length of milling time. The amount of binder needed to prevent cracking depends on the amount of shrinkage, which depends on the amount of brucite developed during the milling and drying time. Because so many of these variables interact with each other, several design of experiments (DOEs) were pursued. Analysis was done using a combination of Minitab (Minitab, Inc, State College, PA) and R (www.r-project.org). Single variable tests were also completed for fundamental understanding. The initial plan for a DOE was a fractional factorial design on MgO concentration, amphiphile type and concentration, binder concentration, and octane fraction. However, early on so many recipes failed to produce stable emulsions that the DOE was abandoned until a working window was established and a more fundamental understanding of the brucite conversion was developed. Afterwards, several more focused DOEs were performed to look at material formulations and processing variables, including the effects of drying and sintering conditions, on the resulting green and sintered porosities.

We found that most formulations that yielded a stable emulsion and that could be dried and sintered without cracking, yielded acceptable ceramics for our application. The variations in parameters that allowed the manufacture of a foamed ceramic were, by and large, too narrow to affect the porosity of the final product in a statistically significant manner, or there was so much

natural variability that we could not determine the relationship between a variable and the response.

We assumed initially that the emulsion drop size would be a key parameter in producing porosity. In the liquid emulsion, the drop size was found to correlate most strongly with the emulsion mixing speed, with much less dependence on the remaining parameters (Figure 20a). The logarithm of the drop diameter *d* exhibited a linear dependence on the mixing speed *v* given by $\log(d) = 4.4155 - 0.0058 * v$. The slope is significantly less than 0 ($p < 0.001$) meaning that there is in fact a relationship between mixing speed and drop size. Despite the fact that variation with *v* explains only about 22% of the variation in *d*, none of the other measured variables were found to have a significant relationship with mean drop diameter, suggesting either a great deal of natural variability in *d* or that there are factors affecting drop size that we have not captured. Notably, above a water phase MgO concentration of 5 vol%, the drop size was not affected by the MgO concentration (Figure 20b). The independence of these two variables is a characteristic of having an excess of particles given the interfacial area (Binks and Whitby, 2004; Sturzenegger et al., 2012), which was also observed in the cryogenic SEM image.

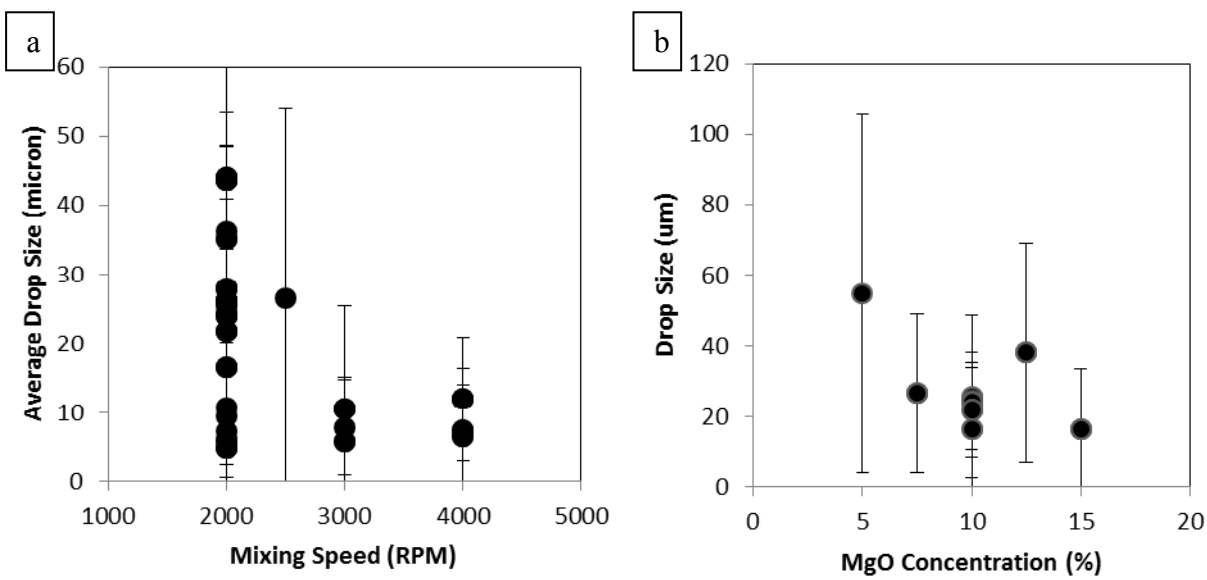

Figure 20a,b: Emulsion drop size as a function of mixing speed and magnesium oxide concentration (vol %) in the water phase. Error bars represent ± one standard deviation of the drop size distribution. For Figure a, the samples were restricted to 10 vol% MgO. For Figure b, the emulsion composition is otherwise the control composition described in the text.

However, surprisingly, droplet size is not a statistically significant factor for estimating porosity (or strength). When the octane concentration was held fixed at 70 vol% of the entire emulsion and the samples were dried slowly, all emulsions that were stable (Figure 15) yielded exceptionally high green porosities (85 – 95 vol%), regardless of recipe or processing conditions. Sintered porosity was more responsive to the recipe variables, specifically the concentration of octane, MgO, and the sintering temperature all have a statistically significant effect ($p < 0.001$) on the sintered porosity. The variable which most strongly affected the total sintered porosity in

the sample was the octane concentration. Figure 21 displays the sintered porosities of all of the Pickering emulsions that were made for the design of experiments. Also plotted in the figure are the porosities of several samples made by drying aqueous solutions of various concentrations of magnesium oxide, omitting any octane, as discussed in the previous section. Thus, samples ranging in porosity between 60% and 90% can be made just by specifying the octane concentration.

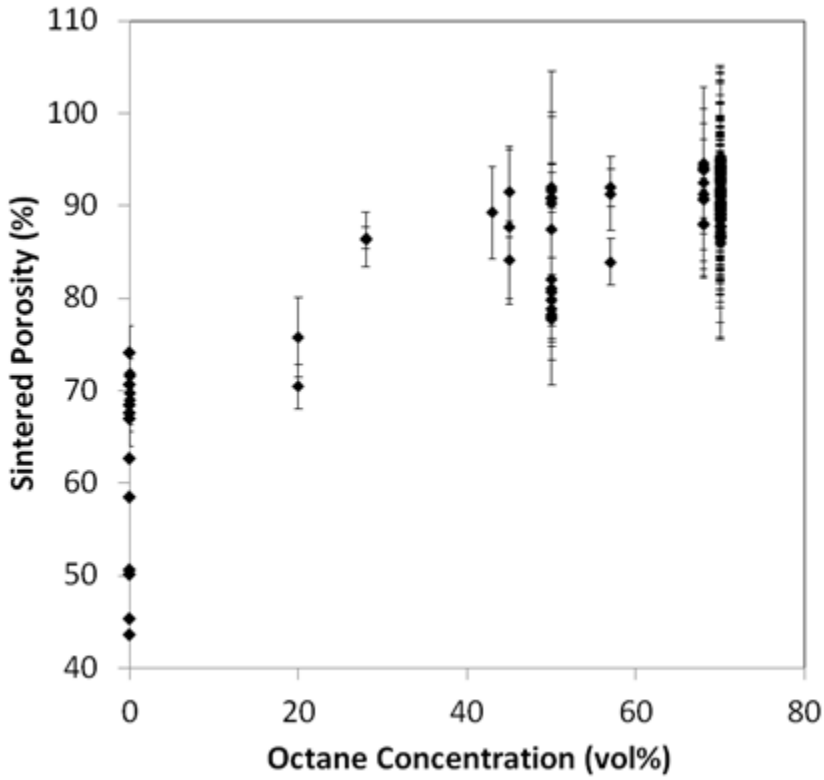

Figure 21. Total porosity of samples containing various concentrations of octane after sintering at 1400 °C. Error bars represent ± one standard deviation of three measurements of porosity for each sample.

As expected, the sintered porosity decreased as the concentration of MgO increased, although this effect was far less profound than the effect of the octane concentration. For example, Figure 22 shows the effect of MgO concentration on the green and sintered mean porosities of samples with otherwise fixed composition consisting of 68-70% octane, 0.01% gellan, and 350 mM Valeric acid, processed in the same manner. Error bars represent the standard uncertainty in the mean from a Student t test at the 95% confidence level. As mentioned previously, magnesium oxide was abundant in the Pickering emulsions, and it is likely that adding excess magnesium oxide also served to increase the MgO in the interstitial spaces between the octane droplets. Amphiphile and binder concentrations had no discernible effect on sintered porosity.

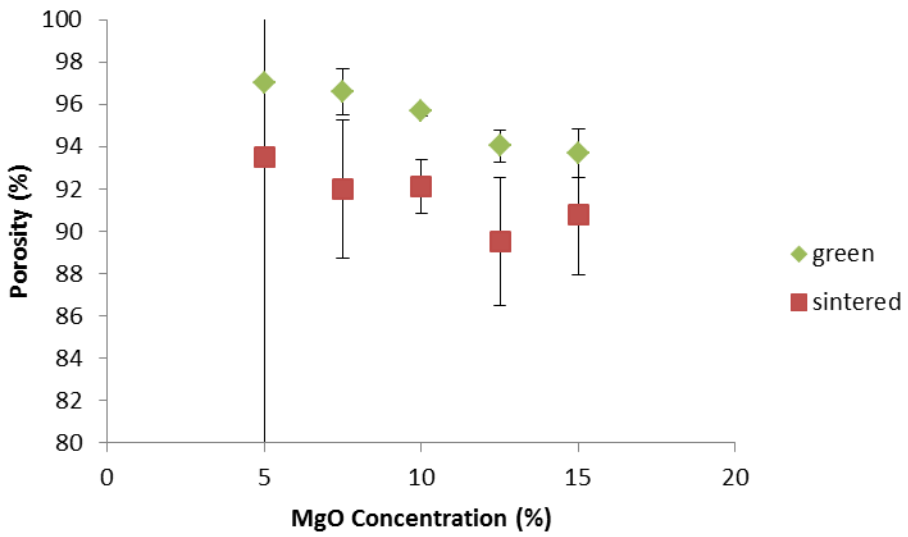

Figure 22. Sample porosity vs. concentration of magnesium oxide in the water phase for samples containing 350 mM valeric acid, 70% octane, and mixed at 2000 RPM. Error bars represent the pooled uncertainty in the mean based on a Student t test at 95% confidence level.

Also, as expected, an increase in the sintering temperature decreased the sample porosity, but again to a much lesser degree than a decrease in Octane or even an increase in MgO. Figure 23 shows the mean final sintered porosity of all samples with a green porosity above 90% decreasing as the sintering temperature increases. Although the average change in porosity between 1300 and 1500 °C is not statistically significant, the trend is downward and confirmed by the statistically significantly lower value at 1600 °C (despite sintering only six samples at this temperature, which increases the uncertainty in the mean).

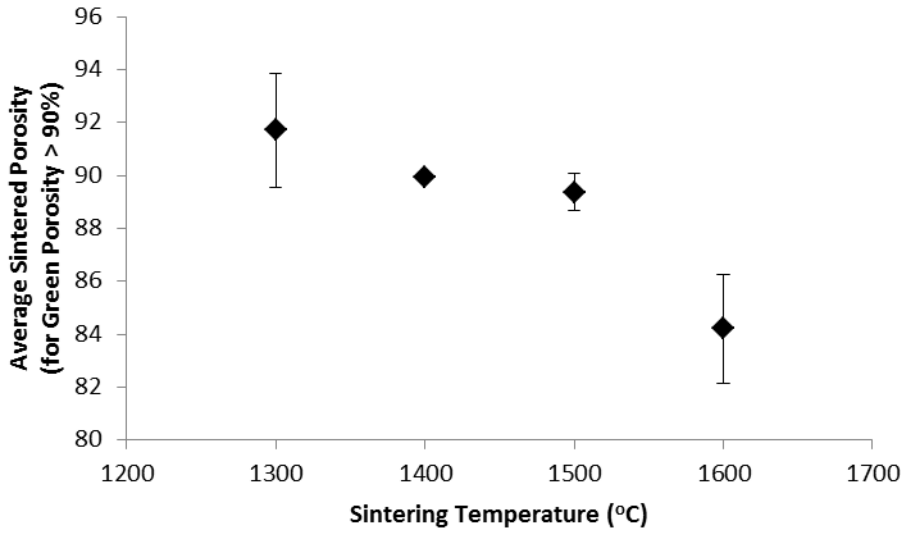

Figure 23. Mean sintered porosity of all samples with a green porosity above 90% when sintered at different temperatures. Error bars represent the pooled uncertainty in the mean based on a Student t test at 95% confidence level.

Finally, in certain cases, the magnesium oxide particles retained a flake-like structure characteristic of brucite even after the samples were sintered (Figure 24). X-ray diffraction confirmed that these sintered samples were only composed of magnesium oxide, and so had been dehydrated completely during the sintering procedure. No correlation between processing parameters and this flake-like structure could be found. However, the microstructure of the magnesium oxide could explain some of the variation in other properties such as porosity or strength. Further investigation into this topic is warranted.

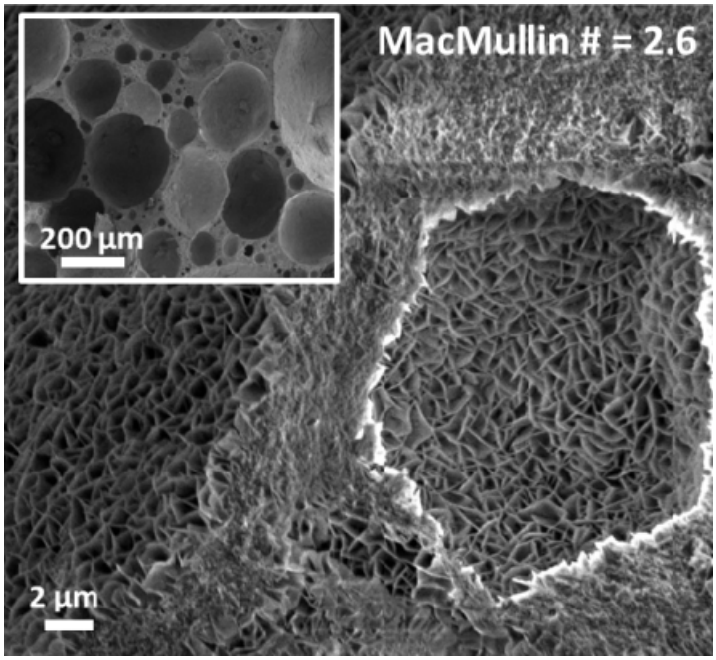

Figure 24. Flake-like structure characteristic of brucite as seen in a sintered Pickering emulsion sample

3.3.4. Pickering Emulsion Separator Performance

In order to properly function in a battery, the separator must be both permeable and able to withstand a compressive force. Electrochemical impedance spectroscopy measurements are used to give a measurement of the permeability through the separator. The impedance is reported in terms of a MacMullin number, or the ratio of the sample impedance to the impedance of the pure electrolyte if it had the same geometry. MacMullin numbers are displayed below in Figure 25 for Pickering emulsions with various connected porosities.

The impedance across a sample has two main contributions: the permeability of the sample as well as its tortuosity. In an ideal case where the tortuosity is not a factor, adding solid will still remove volume available for ion transport. In this case, the MacMullin number is inversely proportional to the porosity ($N_m \sim \phi^{-1}$), which is drawn in Figure 25 as a lower bound for the MacMullin numbers that are possible. Conversely, highly tortuous samples were made by drying aqueous solutions of magnesium oxide as described in the previous chapter. These samples would be comparable to drying the aqueous phase of the Pickering emulsion before octane was mixed in. These samples create an upper bound for the MacMullin number. Most of the Pickering emulsion samples fall between these two extremes, as is expected. Scatter is due to the differing microstructure of each of the samples. For example, factors such as droplet size and foam strut thickness may have no effect on the connected porosity but will have a large effect on the tortuosity of the free paths through the sample. Additionally, samples that retain a flake-like habit after sintering have an improved MacMullin number over those samples that have morphology more characteristic of MgO. This may be because the flakes allow better passage of electrolyte between cavities. Unfortunately, we could find no statistically significant relationship between any processing parameter and the final structure of the sample.

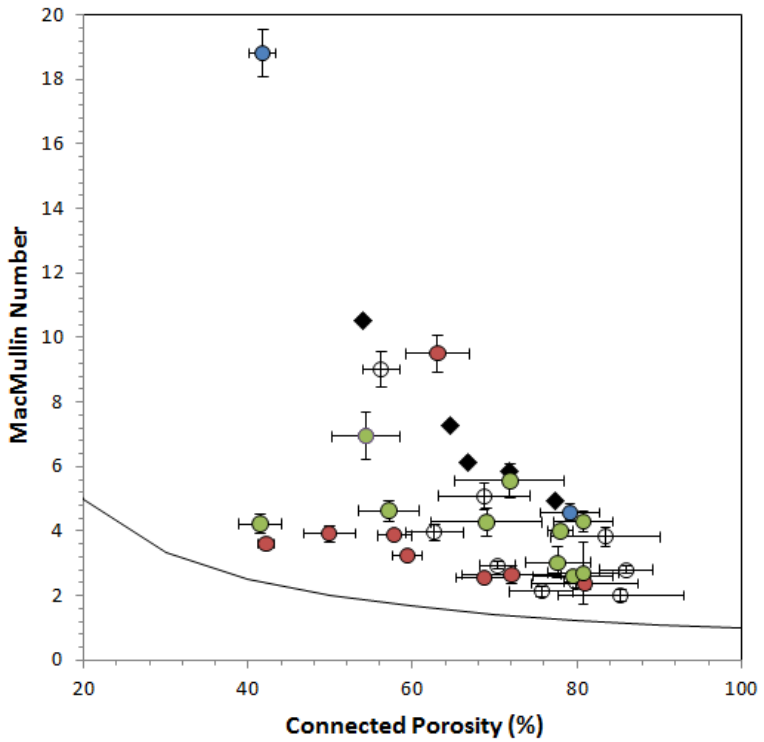

Figure 25: Impedance of Pickering emulsion samples as well as gelled MgO samples not containing octane. An ideal case (solid line) is drawn for samples with nontortuous pore spaces. All circles are Pickering emulsions. Red circles are flake-like, green circles are amorphously shaped (MgO-like), blue circles are odd shaped that fit neither category. Clear circles were not examined with SEM. Black diamonds are gelled MgO samples.

Another measure of the quality of the Pickering emulsions is the compressive force that the ceramic foams can withstand. Force was imposed on a 2 mm diameter post until the top surface of the sintered sample began to fracture. The post diameter was 10-100 times larger than a typical large pore diameter found in the sintered samples, so the fracture force represents the breakage of a large number of foam struts. The fracture force (Figure 26) was found to be highly dependent on the total porosity in the sintered sample. A fit to the data gives the fracture force, $F = 92kg\ (1 - \phi)^{2.3}$. This is consistent with other observations of the compressive strength of closed cell foams, which traditionally scale with a relationship of $(1 - \phi)^2$ (Rice, 1998). Note, however, that 1 kg of force in Figure 26 is equivalent to about 450 psi, so the ceramic foams are still quite strong compared to pressed pellet separators. As is true with the gelled samples discussed in Section 2, the addition of electrolyte salt to the magnesium oxide pore space will further strengthen these samples at room temperature, and it is also unlikely that these ceramic foams will collapse during battery activation.

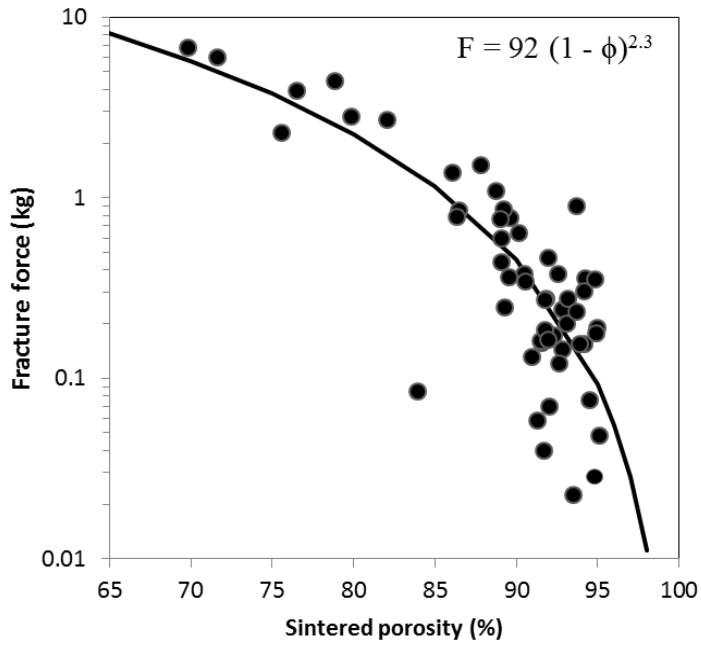

Figure 26: Force required on a 2 mm diameter post to fracture samples of various porosities.

3.4. Conclusions

To increase the porosity dramatically over the gelled magnesium oxide samples of the previous chapter, Pickering emulsions were created by adding up to 70 vol% octane to the dispersion. When dried and sintered, these self-assembled ceramic foams displayed incredible porosities up to 90 vol%. Most processing conditions did not influence the final porosity of the samples with the exception of the amount of octane in the emulsion. By varying the octane concentration, the final porosity of the sample could be tailored to the application. Pickering emulsion samples were found to have improved ionic permeability as compared to gelled MgO samples of similar connected porosity. This is due to the lower tortuosity afforded by the large, open cavities in the Pickering emulsion sample foams. Although Pickering emulsions displayed a lower fracture force than the gelled magnesium oxide samples, in most cases the fracture force was acceptable for battery applications.

4. TRADITIONAL METHODS TO PRODUCE CERAMIC FOAMS

4.1. Introduction

Porous ceramics can be produced through a wide range of processing routes (Colombo & Degischer 2010), including incomplete sintering, sacrificial fillers, and replication. We detail here two primary means we have explored with MgO.

4.2. Methods

4.2.1. Producing Macroporous Reticulated Ceramic Structures Utilizing a Replica Technique

One processing route that was explored to achieve a highly controlled porous structure was utilizing a replica technique, as illustrated in the following schematic (Figure 27).

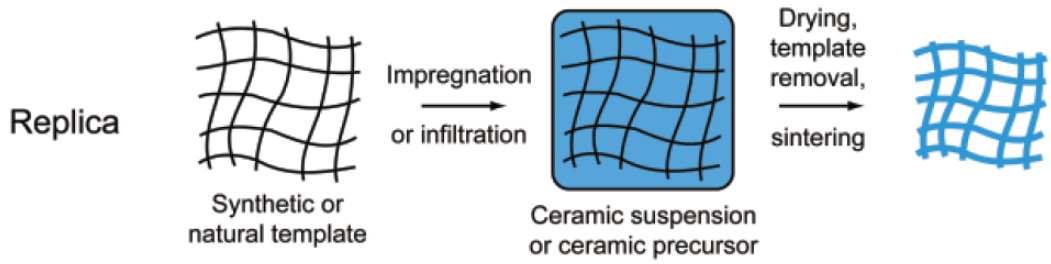

Figure 27. Schematic of replication technique

The method is based on the impregnation of a cellular structure with a ceramic suspension or precursor solution in order to produce a macroporous ceramic exhibiting the same morphology as the original porous material.

Reticulated foam is a highly porous, low density, solid foam ('Reticulated' means like a net). Reticulated foams are extremely open foams i.e. there are few, if any, intact bubbles or cell windows. In contrast, the foam formed by soap bubbles is composed solely of intact (fully enclosed) bubbles. In a reticulated foam only the linear boundaries where the bubbles meet remain. The solid component of a reticulated foam may be an organic polymer like polyurethane, a ceramic or a metal. These materials are used in a wide range of applications where the high porosity and large surface area are needed, including filters, catalyst supports, fuel tank inserts, and loudspeaker covers.

Several different slurries were prepared that involved a 35wt% and 50wt% MgO [Alfa Aesar, Magnesium Oxide, 99.95%, -325 mesh powder] loading mixed into either Ferro B73305 binder system [Solvents: toluene, ethanol, Stoddard solvent; Binder: polyvinyl butyral terpolymer; Plasticizer: dioctyl phthalate; Polymer type: PVB (polyvinyl terpolymer), Binder Solids: 22.4%, Resin:Plasticizer Ratio: 1.7:1, Specific Gravity Solution: 0.88, Viscosity: 450cps] with KD-1

(polyester/polyamine copolymer polymeric dispersant – steric stabilization) [Croda, Hypermer KD polymeric dispersant] or into an elastomeric one-component silicone epoxy resin, Eccocoat SC-3613 [dimethyl, methylhydrogen siloxane, silicone resin]. Both systems worked equally well however the Ferro B73305 binder system was ultimately chosen because it is compatible with a wide range of inorganic powders and coating/casting processes. Hypermer KD polymeric dispersants are composed of one or more anchoring groups, which are adsorbed onto the surface of the ceramic particle, and one or more polymeric chains with a chemical structure designed to provide steric stabilization to the dispersion. Particle-particle interactions are therefore minimized, and this results in lower viscosity and tailored rheology. The resulting slurries were used to impregnate/coat reticulated foam discs of several varying ppi (pores per inch) foam ratings, 20 ppi, 25 ppi, 30 ppi, and 90 ppi, as shown the following images (Figure 28).

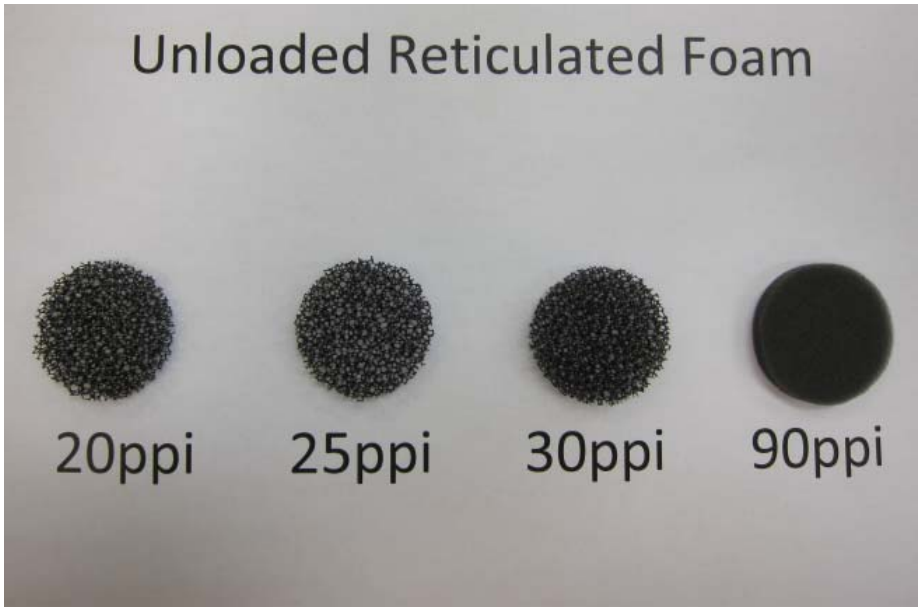

Figure 28. Photo of foam discs used as sacrificial templates to produce foamed ceramics.

The slurry was prepared by ball milling the MgO powder with the Ferro B73305 binder system and KD utilizing a baffled Nalgene bottle and yttria stabilized zirconia milling media. The sacrificial foams were coated with the slurry using a millipore vacuum filtration setup. The uncoated sacrificial foam was placed on a filter screen inside of a beaker funnel attached to a larger vacuum flask. The as-prepared slurry was poured over the foam, submersing it in the slurry, compressed several times and then vacuum was applied to remove the excess slurry from the foam. The coated foam piece was then allowed to air dry in a fume hood and eventually moved into a drying oven, for approximately 24 hours. The dried and coated foam preforms were then placed on alumina sand and furnace setters for sintering. The MgO impregnated foam discs were then fired at 1600°C with a 2 hour isothermal hold. The organic template decomposes during sintering, leaving the ceramic replica. Images of the resultant sintered replicas can be seen in Figure 29 and Figure 34.

Figure 29. MgO ceramic discs made with a foam replication technique.

4.2.2. Producing Macroporous Ceramic Structures Utilizing a Sacrificial Poreformer and Tape Casting

Tape casting is a straightforward method of forming uniformly thin sheets of film that is inexpensive, scalable, and may be used with any ceramics, metals, or polymers that are readily mixed in a liquid suspension or slip. Developers who successfully produce prototypes on a bench tape caster can be confident that similar results will be reproduced on larger-scale production machines. The feed stock for the tape casting process is a slip made from a suspension of ceramic, metal or polymer particles in an organic solvent or water, mixed together with strengthening plasticizers and/or binders. The actual tape is formed when the slip is cast onto a flat surface by doctor blade to a carrier film or steel belt.

Porous MgO discs were prepared utilizing a sacrificial poreformer, polytetrafluoroethylene (PTFE) [Shamrock Technologies, Inc., MicroFLON 124-T4, mean particle size = 16-30 μm with a D90 of 40 μm and a specific surface area of 1-3 m^2/gram], MgO [Alfa Aesar, Magnesium Oxide, 99.95%, 325 mesh powder] and Ferro B73305 binder system [Solvents: toluene, ethanol, Stoddard solvent; Binder: polyvinyl butyral terpolymer; Plasticizer: dioctyl phthalate; Polymer type: PVB (polyvinyl terpolymer), Binder Solids: 22.4%; Resin:Plasticizer Ratio: 1.7:1; Specific Gravity Solution: 0.88; Viscosity: 450 cps] with KD-1 (polyester/polyamine copolymer polymeric dispersant – steric stabilization) [Croda, Hypermer KD polymeric dispersant]. This binder system utilizes polyvinyl butyral (PVB) resins and toluene-ethanol blends of solvents and it is designed for use directly in a mill for dispersion only, no addition of plasticizers or dispersants is required as they are contained in the binder solution. In order to improve the slip characteristics, KD-1 was added as an additional steric stabilizing surfactant dispersant.

Several volume percent loadings of poreformer were prepared for comparison, including, 40 vol%, 50 vol%, and 70 vol% (percent ratio of total poreformer to total poreformer and total

MgO). The MgO and poreformer in the desired ratio was milled in a baffled Nalgene bottle with 5mm diameter YSZ (yttria-stabilized zirconia) milling media and toluene using a turbula mixer. The milled mixture was then added to a pre-mix of the binder system, dispersant and milling media, 10mm diameter YSZ milling media, in a baffled Nalgene bottle and ball milled for at least 72 hours on a roller mill. The ball-milled slip was then passed through a three roll mill (Gap 1 = 130µm, Gap 2 = 5µm, RPM = 500 at 9:3:1 turn ratio), filtered through a sieve, and de-aired in a vacuum chamber. (Note: The higher volume percent loaded slip, 70vol%, was cast without three roll milling and de-airing).

The slip was then tape cast using a 14" wide aluminum double doctor blade fixed on a granite surface plate (HED International Inc., Labcast table top tape caster, Model TC-71LC) (Figure 30). The underbed temperature controller and air-heater controller were set and maintained at 30 °C. The slip was tape cast onto a silicone coated Mylar substrate using a doctor blade gap thickness of 356 µm for the reservoir blade and 279 µm for the casting blade at 50% speed setting (10 cm/min). The initial dry green thickness of the tape was approximately 80-90 µm.

Lab-Cast Model TC-71LC

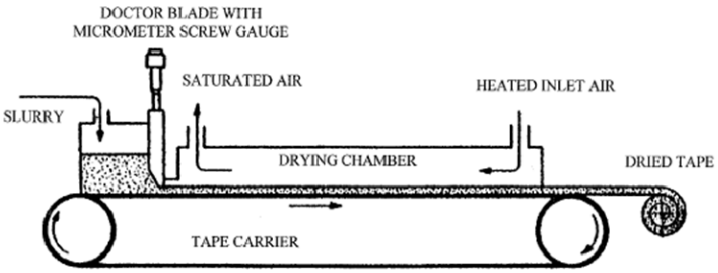

Figure 30. Photo (left) and schematic (right) of tape casting system.

The dried green tape was cut into 3" wide strips and then into 3"x3" square sheets and stacked into 6, 8, and/or 10 layer packets. The packets and individual layers were sandwiched between sheets of 75 µm thick Teflon-coated Mylar and two layers of 225µm thick Mylar and vacuum sealed in a plastic bag. These packets were then warm platen uniaxial pressed (Carver Inc., Model-CHC, 12 ton hydraulic laboratory press with heated/cooled 6"x6" platens) to 85 °C at 2400lbs force, rotated 90° and then re-pressed a total of four times to produce a uniformly laminated substrate, an image of the stacked and laminated substrate can be in Figure 31.

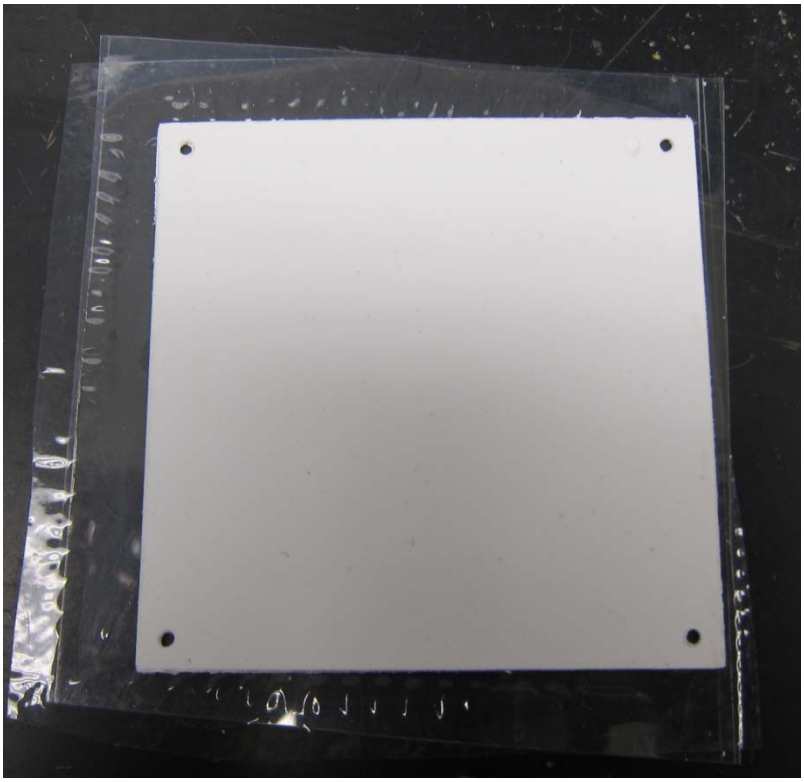

Figure 31. Laminated substrate formed from stacking and pressing layers of green ceramic tape.

The green laminated substrate was then removed from the packet and diced into four 1.5”x1.5” square samples. Initially these final green laminates were pyrolyzed in a low temperature drying oven (to approximately 300 °C, in approximately 72 hours) to allow for the gradual decomposition and diffusion of the polymeric material, and avoid the build-up of pressure within the laminate and bloating. Eventually though, a more involved thermal profile was developed to allow for direct pyrolysis and sintering in a high temperature furnace. In order to maintain a required level of flatness and parallelism for the discs, based on the end application requirement, a specially designed setup was developed for pyrolysis and sintering. The green laminates were sandwiched between 1.5”x1.5” plates of MgO that were machined flat and dusted with MgO powder to prevent adhesion during sintering. This setup was then covered in MgO powder in order to baffle the heat transfer from the furnace to the parts. The images below illustrate this setup and procedure (Figure 32).

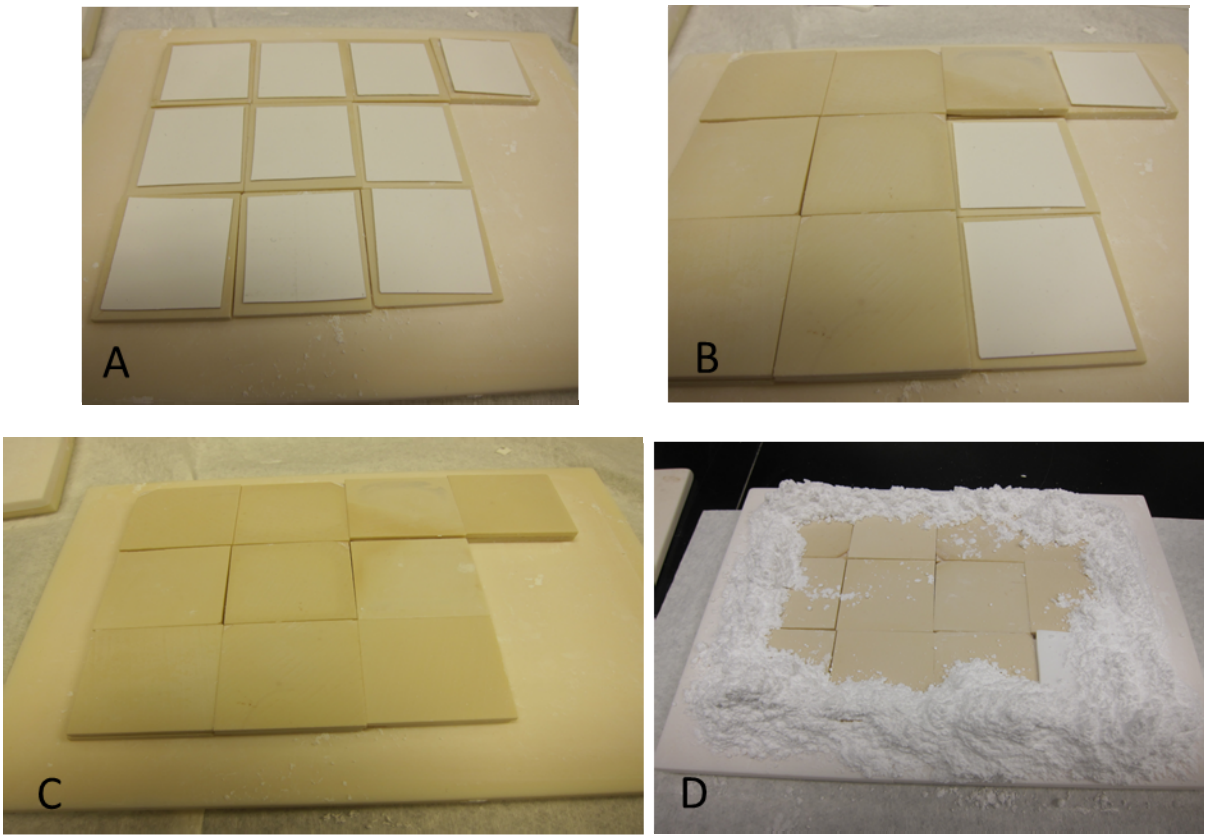

Figure 32. Steps to prepare laminates for sintering showing (A-C) them sandwiched between flat plates of MgO and (D) dusted with MgO powder.

MgO samples were laser cut with a 400 Watt 1060nm EDI CO_2-Laser; model G-150 (Tucson, AZ). Each sample was placed onto a sheet of 0.010-in thick alumina (ADS-96R, from Coorstek, Grand Junction, CO), which acted as a support while the MgO samples were being machined. Each sample was cut with the following laser parameters: 9000 µs pulse period, 150-200 µs pulse width (depending on the thickness of the sample), 0.080 in/sec feed rate, and air pressure of 5 psi. The laser beam was focused on the top MgO surface (±0.005 in depending on the sample). The green MgO samples were processed in the same manner except the pulse width was 25-50 µs.

We also briefly explored the addition of punched holes to MgO tape (without poreformer) to create structures that allow a direct line of electrolyte to form between cathode and anode. Green tape was punched in regular arrays and then sintered (Figure 33). However, it was quickly realized that holes could not be spaced closely enough to produce a highly porous sample, even after shrinkage during sintering. The ability to create holes small enough to retain the electrolyte was also problematic.

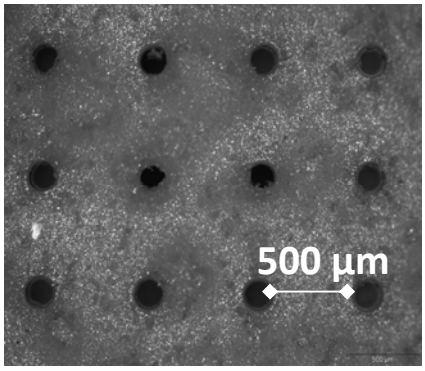

Figure 33. Sintered tape cast with a punched hole array

4.3. Results

4.3.1. Replication Technique

Figure 34 shows close-up photos of a reticulated foam made with a 25 ppi template. The foam nature of the sample gives exemplary connected porosity and low MacMullin numbers (as will be shown in Figure 38). These reticulated foam samples, although very porous, contained comparatively large pores that did not hold the aqueous salt solutions well. Although not reflected in Figure 38, over time, during testing, the conductance of the samples would degrade due to draining of the liquid. Furthermore, it was feared that the large pore sizes of the reticulated foam samples would prevent thin separators from being constructed. Although templates with much smaller pores (90 ppi) were later obtained, processing using these templates was not optimized by the time we were ready to backfill ceramics with electrolyte (Section 5) and produce samples for single cell testing (Section 6).

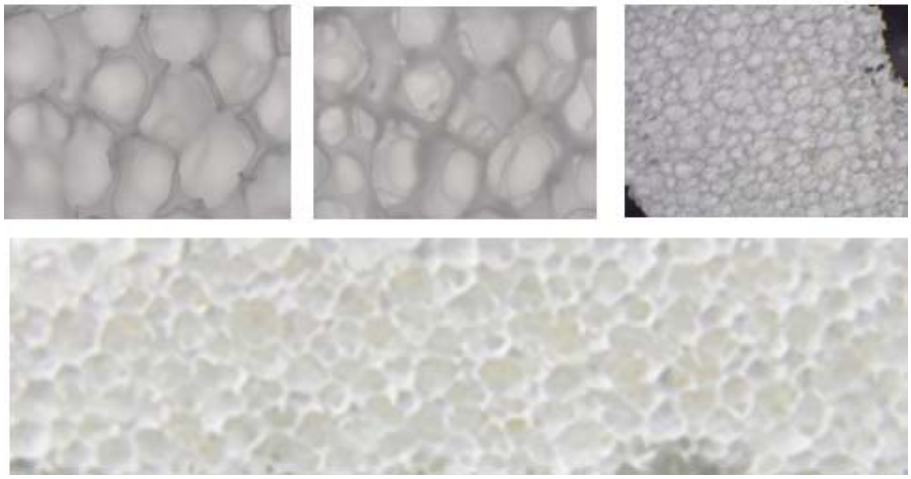

Figure 34. Images of MgO ceramics made with a foam replication technique.

4.3.2. Tape Casting with Addition of Poreformer

Figure 35 shows an SEM image of a sintered pellet produced with tape casting an MgO slip with the addition of 40 vol% PTFE poreformer. Although the tortuosity of the sample appears large, reasonable porosities could be produced (Figure 36) as well as good MacMullin numbers (Figure 37). The pores are small and, therefore, the material retains the electrolyte well.

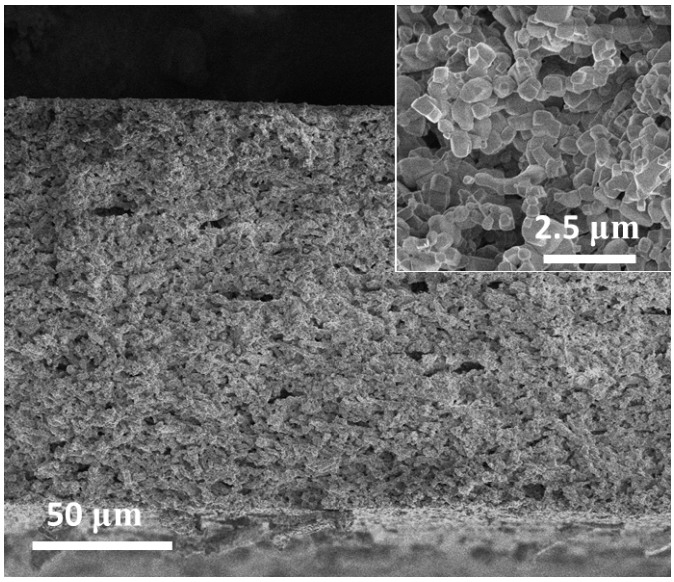

Figure 35. SEM image of a cross section of a 40% PTFE poreformer sample

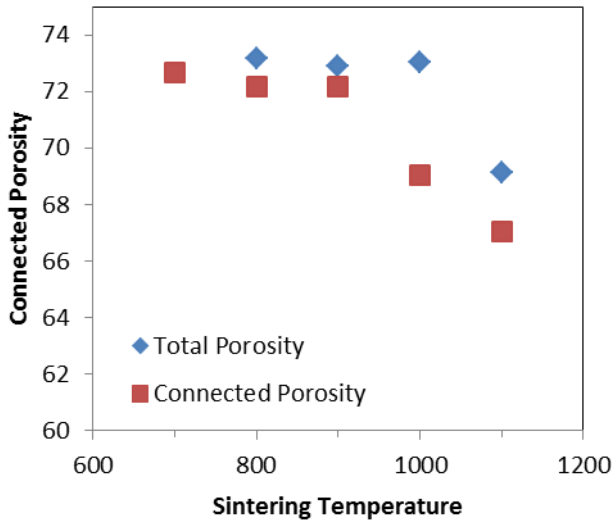

Figure 36. Sample porosity for 10 layer PTFE poreformer samples sintered at various temperatures

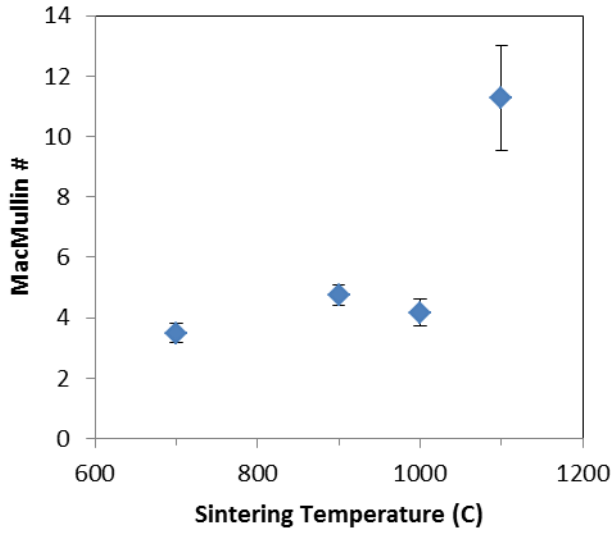

Figure 37. MacMullin number for 10 layer PTFE poreformer samples sintered at various temperatures

5. COMPARISON OF DIFFERENT METHODS AND DOWNSELECT

To choose which MgO separator fabrication procedures would be targeted for future development, the sample strength and permeability were used as selection criteria. Figure 38 displays MacMullin numbers measured for six different sample types, measured with aqueous KCl salt solutions as previously described. In most cases, the connected porosity describes the permeability through the sample, despite the effects of microstructure. Compressive strength values (Figure 39) were also well described by the overall porosity for all sample types.

From these results, the reticulated foam samples were excluded from further testing as discussed in the previous section. Punched tape samples were also excluded. Although the tortuosity of the pores in these samples was very low, the overall porosity was also comparatively low. Consequently, ionic transport was limited in these samples and the MacMullin numbers were very high.

The samples that showed the most promise, with MacMullin numbers around 5, were Pickering emulsions, gelled magnesium oxide samples, and poreformer tapes. These samples also displayed acceptable compressive strengths. Therefore, these samples were targeted for electrolyte filling methods.

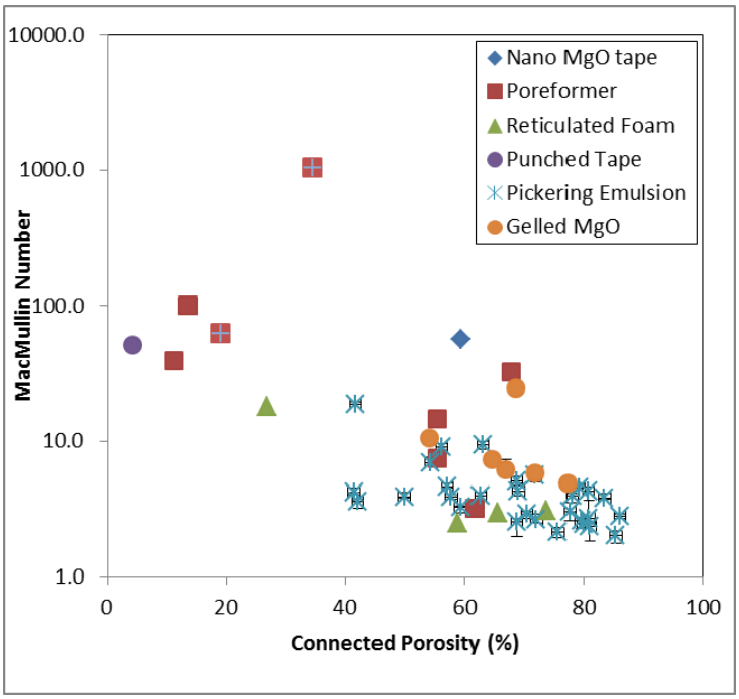

Figure 38. Impedance values for all sample types

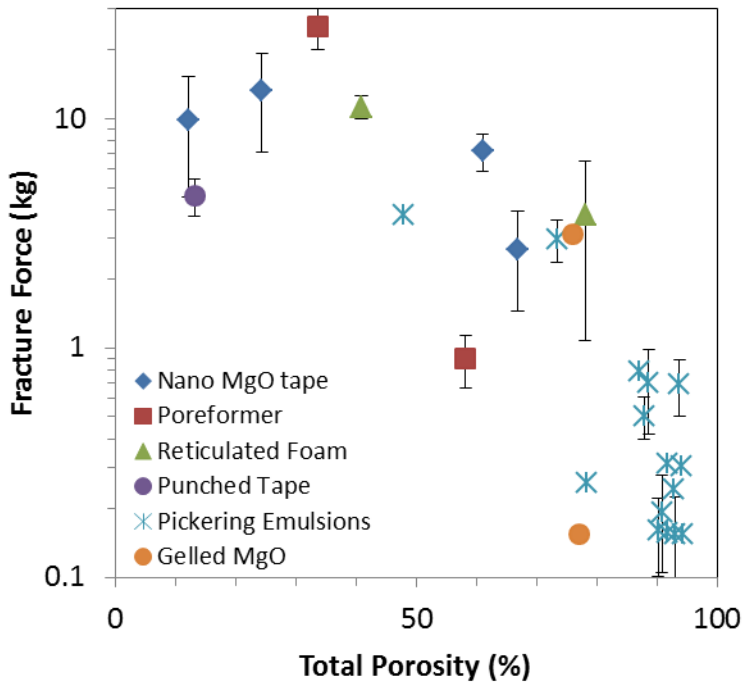

Figure 39. Strength values for all sample types

6. FILLING CERAMIC SCAFFOLDS WITH THERMAL BATTERY ELECTROLYTE

6.1. Introduction

In the traditional pressed pellet technology, salt and magnesium oxide powders are pressed together into separators directly. However, the new MgO structures proposed here are first sintered into a porous network. Although the sintering step is advantageous in terms of sample strength, the LiCl/KCl eutectic salt, which melts and even volatilizes well below the MgO sintering temperature, must be added to the separator in a post-processing step. Therefore, new methods of adding salt to the MgO network had to be developed for Pickering emulsions, gelled tape cast samples, and poreformer tape cast samples.

6.2. Methods

6.2.1. Dipping into melted eutectic salt

The first filling method attempted was to dip the samples directly into the melted salt. Upon removal, the salt would freeze in the sample pores.

The inside of a glass beaker was coated with boron nitride (BN) to protect it from chemically reacting with the melted LiCl/KCl eutectic salt. Salt (LiCl KCl eutectic, Sigma Aldrich) was melted in this container by placing the beaker on a hot plate within a glove box. The argon glove box atmosphere prevented moisture (0.6 ppm) or oxygen (0.3 ppm) from reacting with the melted or room temperature salt. The temperature of the salt was monitored using a K-type thermocouple. The salt melts at 352 °C.

Initially the salt was heated to 400 °C. Samples were either dropped into the bath, dipped into the bath slowly using tweezers, or dipped into the bath with tweezers after partially preheating the samples. A nickel mesh basket was also made to dip the samples into the salt in a “belly flop” orientation. In all cases, tape cast poreformer samples (8 layer, 40% poreformer, h = 0.7 mm) broke during the process. Approximately half of the samples cracked on first contact with the salt, whereas the other samples cracked on solidification of the salt after removing the samples from the salt bath. In all cases, the boundary between the wetted and non-wetted portion of the sample was a weak point in the sample. Therefore, it was hypothesized that the thermal expansion of the magnesium oxide network created a thermal stress mismatch between the hot and cold halves of the sample. Upon cooling, additional stress was introduced by the cooling, freezing, and shrinkage of the salt. Gelled magnesium oxide samples also broke during this filling process, whereas Pickering emulsion samples were only partially filled. Pickering emulsion samples still contained approximately 60 vol% porosity after the filling process. Because of these challenges, this method was not pursued further.

6.2.2. Filling with LiCl/KCl aqueous solutions

The second filling method was to dry aqueous solutions of the LiCl/KCl eutectic in the porous network, leaving only the salt behind. Saturated solutions of the salt were prepared at room temperature in Milli-Q purified water. The aqueous solutions were then dripped onto the top of the ceramic samples, which had previously been baked at 500 °C to clean off any accumulated water or organics. To draw the solution into the pores of the network a vacuum was pulled on the wet samples and the temperature was increased to 30-40 °C to dry the water away. During this process, the separators were propped up on tripods or rings to keep salt crystals from adhering the samples to the vacuum oven floor. The filling procedure was repeated 6-8 times, each time taking care that the solution never dripped through the samples, which could wash away the previous salt depositions.

Using this method, samples did not crack during the filling process. However, the amount of electrolyte added to the pore space was very inconsistent even for copies of the same sample. Dried salt filled 19-77% of the original porosity of gelled MgO tape cast samples, with most samples measured to be 30-40% filled. Poreformer samples behaved similarly. Fill variability could be caused by aqueous salt solutions leaking through the sample disks as they were filled, or sections that were well filled may have blocked unfilled areas in an inconsistent manner. Furthermore, the fill percentage was very difficult to measure since many samples had a crust of excess salt on top that could not be chipped off completely without breaking the fragile separators. Thermogravimetric analysis measurements showed that the eutectic composition of the salt was preserved in the final dried samples.

Although salt did fill the spaces between individual MgO particles in Pickering emulsion samples (Figure 40), the larger cavities originally occupied by the octane droplets did not fill. This is likely because the water solution wet the highly curved small pores more easily than the larger pores. It may have been that access to some of the larger pores was closed off when the smaller pores were filled. Due to the large amount of porosity left unfilled, this method was not considered successful for filling Pickering emulsion samples.

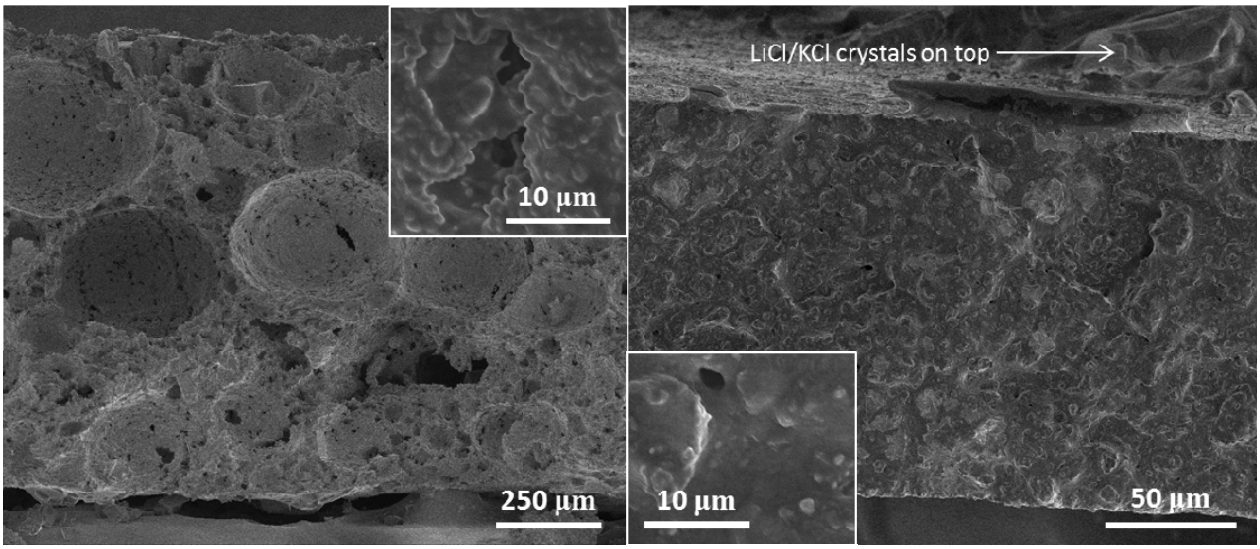

Figure 40. SEM images showing cross sections of a Pickering emulsion sample (left) and a poreformer sample (right) filled with salt using the aqueous solution method

6.2.3. Gradual temperature increase

Because samples tended to crack under fast temperature changes, another filling method was devised where salt would be placed on top of a sample and the temperature gradually increased until the salt melted and filtered into the porous structure. The sintered and laser cut porous MgO substrates (approximately 25.50 mm diameter by 0.55 mm thick for tape cast samples and 25.50 mm diameter by 1.15-1.80 mm thick for emulsion samples) were set on a thin bed of alumina sand (1mm particle size alumina) inside of an alumina dish. Research grade salt LiCl-KCl eutectic mixture was used to load on top of the porous MgO substrates (approximately 0.40 grams for the 0.55 mm thick samples and varying amounts for the thicker samples, based on a nominal 70 vol% theoretical amount). The alumina dish was then covered with an alumina plate and placed inside a box furnace. The optimal thermal profile, based on this configuration, was room temperature to 475 ^{o}C at 5 ^{o}C/min, hold at 475 ^{o}C for 60 minutes, and then 475 ^{o}C to room temperature at 10 ^{o}C/min. In most cases the substrates did not adhere to the underlying alumina sand, however, higher salt amounts would typically result in an increased amount of molten salt flow through the porous MgO substrate. This was problematic on cooling and solidification making when it became more difficult to remove the substrates from the alumina.

The gradual temperature increase filling method consistently filled 85-100% of the available porosity for both gelled MgO and PTFE poreformer samples. Again, exact amounts of salt were difficult to measure since many samples had excess salt left on top. Early tests with the Pickering emulsion samples, however, showed that the samples were not wet by the melted salt (Figure 41). After the melting and cooling process, the salt remained completely on top of the sample. Since Pickering emulsions are fabricated from the same magnesium oxide (Fisher) as the gelled MgO samples, wetting differences cannot be due to impurities in the ceramic. Instead, it is likely that the vastly different pore size in the Pickering emulsion samples caused the

difference in the wetting behavior. However, these tests were preliminary and wetting agents may help backfill the ceramics from Pickering emulsions.

Figure 41. Electrolyte salt does not wet Pickering emulsion samples. Salt was melted in a vacuum furnace, cooled, and removed to the atmosphere.

6.2.4. Conclusions

Of the three filling methods, the most reliable one for adding the most salt to the porous structure was the gradual temperature increase. However, the aqueous filling technique also produced many samples with large amounts of electrolyte. Unfortunately, to date no acceptable method was discovered for Pickering emulsion samples. Although the Pickering emulsions have the most porous structure of all three ceramics, without a better method to fill them with electrolyte they are not contenders for thermal battery separators. Wetting agents may help achieve reasonable fill rates.

It was observed, but not quantified, that the pellets were stronger and less susceptible to breakage during handling once filled with electrolyte. As will be seen in the next section, underfilled samples could still break when stacked to produce a battery cell, but we also observe that those samples that broke were not as flat as samples produced nearer the end of this project.

7. SINGLE CELL TESTING

7.1. Test Procedure

For single cell tests, stacks were made containing one cathode, one anode, and a separator, with dimensions shown in Table 1. Pellets were specifically pressed for these tests, and although not taken from an existing battery design, they are representative of those in actual batteries. The anode was not flooded with electrolyte. The separator was 35wt% MgO (Merck MagLite S) and 65 wt% LiCl-KCl eutectic electrolyte, where the eutectic is 45 wt% LiCl and 55 wt% KCl. The cathode was 73.5 wt% FeS_2, 25 wt% separator mixture, and 1.5 wt% Li_2O. A stainless steel current collector was placed on either side of the single cell stack and the entire stack was sandwiched with sheets of mica.

Samples were discharged between heated metal platens within a dry and oxygen free glove box. An 8 psi compressive pressure was added axially to the single cell during the test to simulate the expected pressure that the cell would experience in an activated battery. An Arbin Instruments BT2000 battery tester was used to apply either a constant current or a pulsed current load and monitor the resulting battery voltage. The constant current test consisted of an open circuit voltage hold for 60 seconds followed by a 50 mA/cm^2 discharge until the battery voltage was less than 0.5V. The pulse tests also started with a 60 second open circuit voltage hold followed by a current load of 50 mA/cm^2. Every two minutes the load is removed for 30 seconds, pulsed to a 200 mA/cm^2 load, rested at the open circuit voltage, and then returned to the medium load of 50 mA/cm^2. These current profiles are illustrated in Figure 42. In both cases, the tests were stopped when the voltage of the single cell dropped below 0.5 V for any current load.

Table 1. Single Cell Pellet Dimensions

	Material	Diameter (in)	Thickness (mm)	Mass (g)
Cathode	FeS_2 /Separator material	0.999	0.62	0.745
Separator	LiCl-KCl eutectic/ MgO	1.01	0.42	0.394
Anode	LiSi	0.999	0.92	0.395

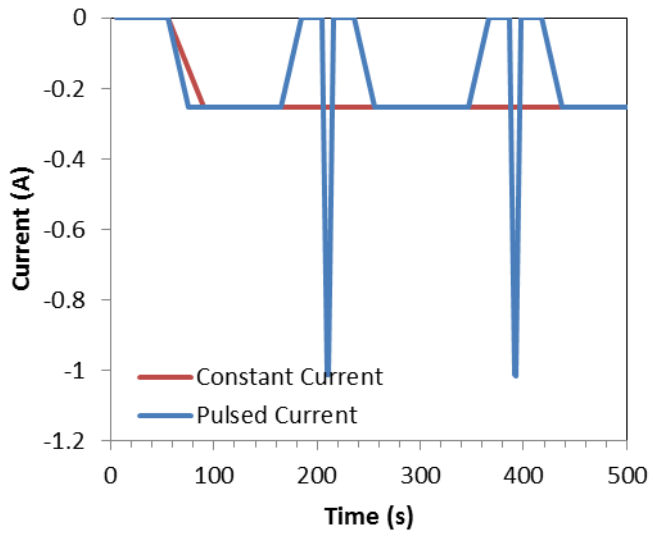

Figure 42. Constant current and pulsed current load profile for 1 inch diameter pellets

7.2. Performance of traditional pressed pellet technology

In order to compare the sintered separator performance to the traditional pressed pellet technology, first the performance of the pressed pellets was needed to be evaluated for the given pellet dimensions and chemistry. Single cell voltage curves were obtained for temperatures ranging from 400 °C – 500 °C (Figure 43 and Figure 44).

Constant current voltage curves consist of a voltage plateau at 1.9 V which then decays to a second, lower voltage plateau. Each plateau corresponds to a chemical reaction that takes place in the cathode. Most batteries are designed to operate only during the first transition (FeS_2 reduction to $Li_3Fe_2S_4$). At 450 °C and 500 °C the reaction proceeds fully. At 400 °C, however, the battery voltage decays prematurely. As the battery discharges the separator electrolyte gains lithium, pushing the salt concentration away from the LiCl/KCl eutectic. Non-eutectic salt mixtures melt at higher temperatures; it is likely that 400 °C is too low of a temperature to keep the electrolyte molten during the battery discharge.

Voltages collected during the pulsed current loads show the same cathode transitions. During the current pulses, the voltage drops according to the cell resistance. At lower temperatures, the cell resistance is higher during the initial plateau. This is remarkably true at 400 °C, where it is likely that portions of the cell are freezing during the discharge.

From these data, it was decided that further discharge tests of single cells made from experimental separators would be performed at 500 °C.

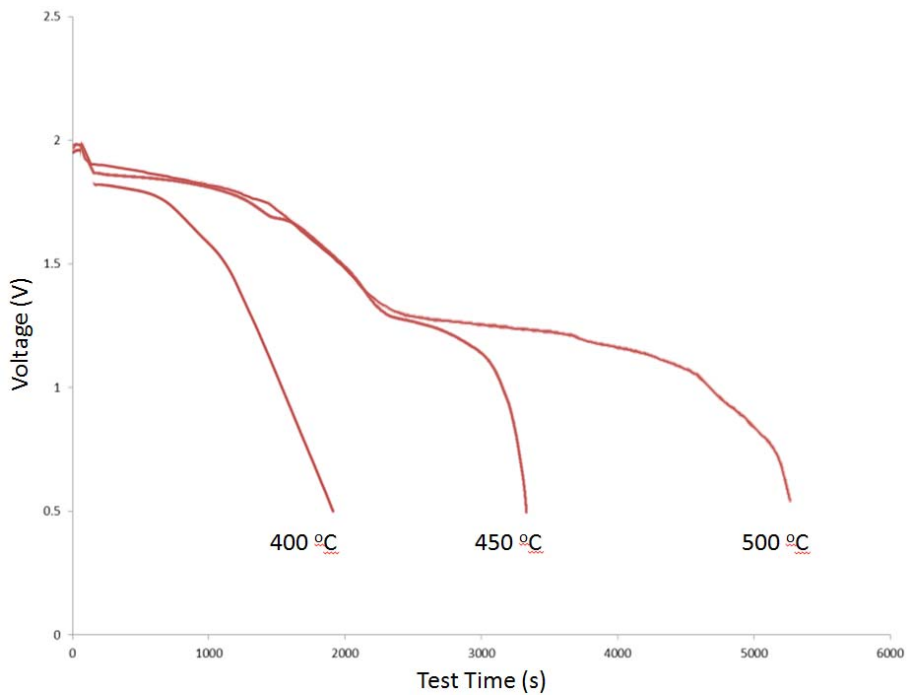

Figure 43. Voltage of single cells composed of 1 inch diameter pressed pellets under a constant current load of 50 mA/cm2

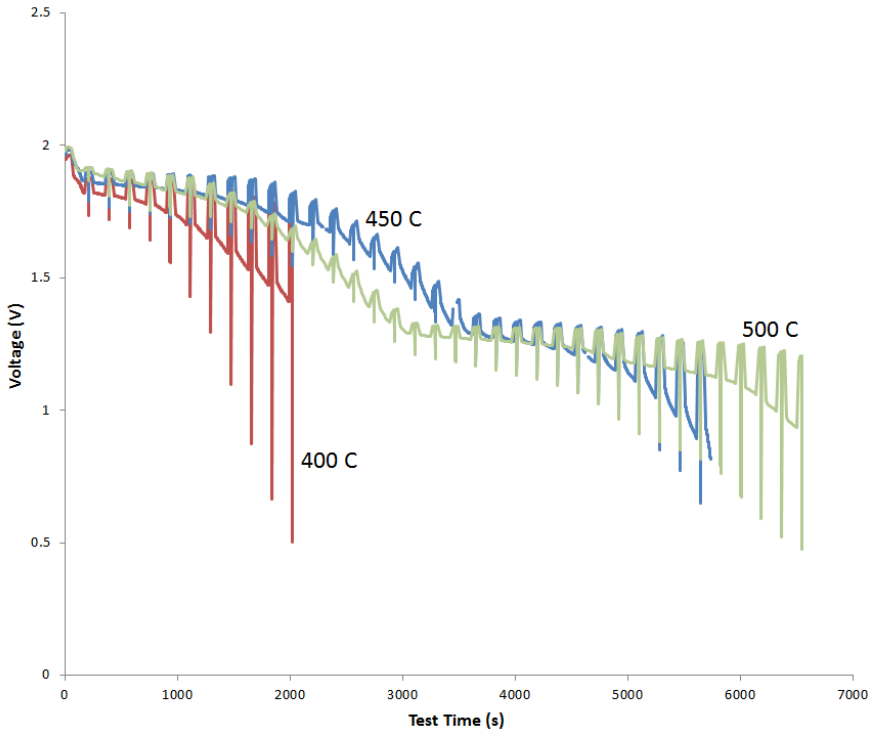

Figure 44. Voltage of single cells composed of 1 inch diameter pressed pellets under a pulsed current load

7.3. Performance of sintered separator thin film technology

7.3.1. Gelled MgO samples

Preliminary single cell testing was performed for three samples of gelled MgO samples. These represent a "worse-case" scenario because the filling method was based on filling with aqueous solutions of the LiCl/KCl eutectic salt as described in section 6.2.2. Thus the amount of electrolyte was less than was later accomplished with melting the salt as described in section 6.2.3. Testing of the latter method with the gelled samples was not complete by the time of this publication.

Table 2 defines the characteristics of two gelled MgO separators as well as that of the traditionally pressed pellet (E1C). Figure 45 shows the voltage output as a function of the cathode capacity. Pellet TC28 performs well despite having a lower volume of electrolyte. The first plateau extends farther than that of the cell using a traditional pressed separator. We speculate that the dry anode used in these tests may have wicked out the available electrolyte in the thinner sample TC20.

Table 2. Gelled MgO separators tested in a constant current single cell battery

ID	Notes	Filling method	h (mm)	Before fill	After filling		
				Total porosity	vol% MgO	vol% elect	vol% pores
TC28	12.5% MgO	LiCl/KCl aqueous	1.39	84	16	30	53
TC20	12.5% MgO + gellan	LiCl/KCl aqueous	0.67	73	27	47	27
E1C	vol%s after melting	Pressed pellet	0.42		20	80	0?

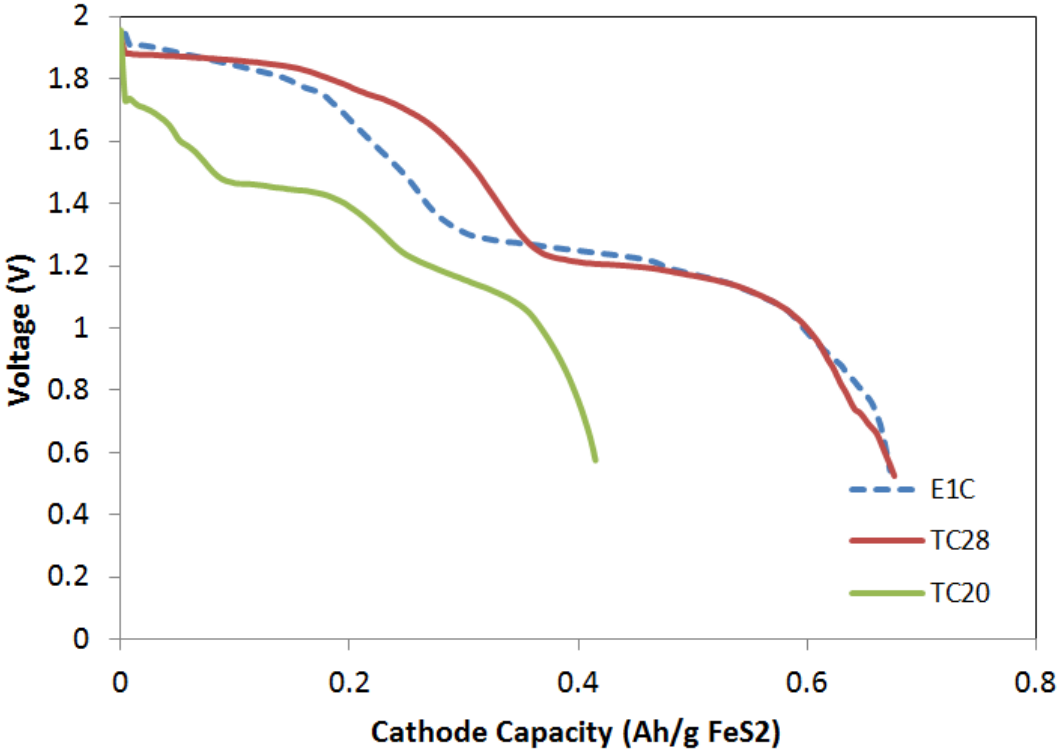

Figure 45. Voltage of single cells composed of an anode, cathode, and 1 inch diameter gelled MgO separator, compared to a pressed pellet (E1C) under a constant current load of 50 mA/cm^2

Results using a pulsed current load are shown in Figure 46, with the pellets defined in Table 3. Here, TC48 and TC51 clearly failed, most likely because they were not perfectly flat. However, TC39 performed well. The resistance of the cell is reflected in the depth of the pulses. Note that at early times (where the useful life of a battery is designed to occur) the resistance of the gelled sample is not significantly larger than that of the cell using an E1C pellet. Later on the first plateau the resistance is greater with the gelled sample however; although, again the plateau lasts longer.

Table 3. Gelled MgO separators tested in a pulsed current single cell battery

ID	Notes	Filling method	h (mm)	Before fill	After filling		
				Total porosity	vol% MgO	vol% elect	vol% pores
TC39	12.5% MgO + gellan	LiCl/KCl aqueous	0.97	84	22	37	41
TC48	17.5% MgO, extra salt on top	LiCl/KCl aqueous	0.466	63	37	80	-17
TC51	17.5% MgO, sample not flat	LiCl/KCl aqueous	0.453	68	32	35	33
E1C	vol%s after melting	Pressed pellet	0.42		20	80	0?

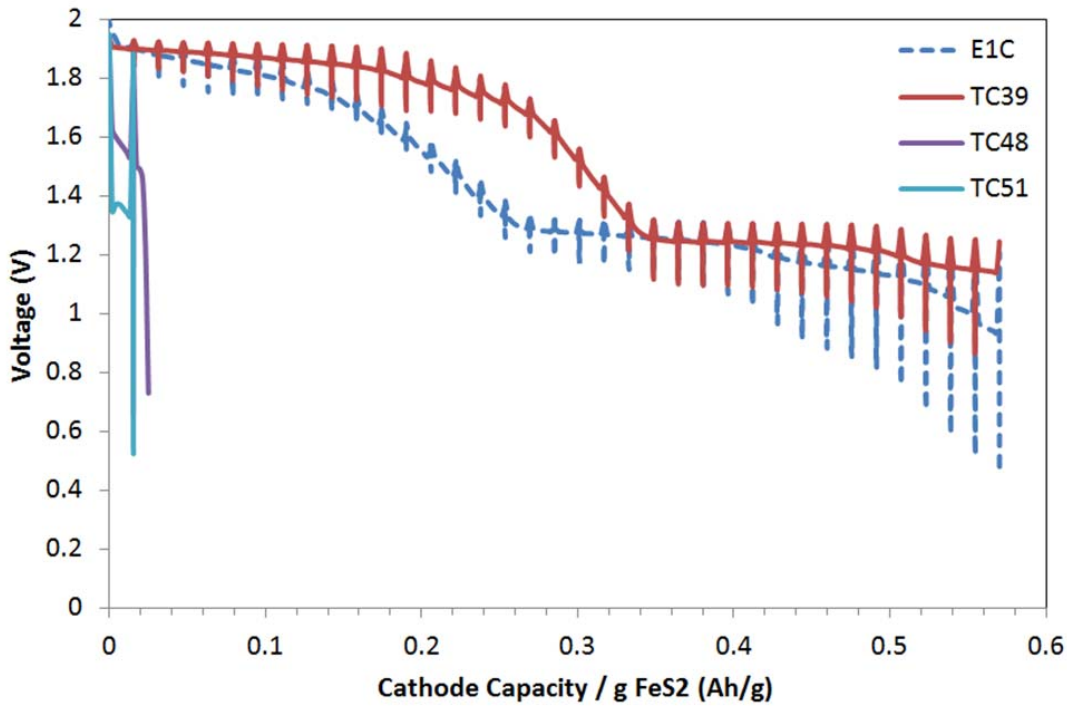

Figure 46. Voltage of single cells composed of an anode, cathode, and 1 inch diameter gelled MgO separator, compared to a pressed pellet (E1C) under a pulsed current load.

7.3.2. Poreformer tape

Preliminary single cell testing was also performed for six samples of poreformer-based ceramic separators. Here, several filling method were based on filling with aqueous solutions of the LiCl/KCl eutectic salt as described in section 6.2.2 (samples CT64-CT40 in Table 4). Samples KM78 and CT115 were filled by melting the salt as described in section 6.2.3.

Figure 47 shows the voltage output as a function of the cathode capacity. Pellet CT115 performs the best, not surprisingly because the volume of electrolyte is the highest. This method of filling was adopted later as the best based on these results. Again the first plateau extends farther than that of the cell using a traditional pressed separator.

Table 4. Poreformer tape separators tested in a pulsed current single cell battery

ID	Notes	Filling method	h (mm)	Before fill	After filling		
				Total porosity	vol% MgO	vol% elect	vol% pores
CT64	40% poreformer, 700°C sinter	LiCl/KCl aqueous	0.59	73	27	22	51
CT69	40% poreformer, 1000°C sinter	LiCl/KCl aqueous	0.55	69	31	23	46
CT74	40% poreformer, 900°C sinter	LiCl/KCl aqueous	0.8	73	27	20	53
CT40	40% poreformer, 900°C sinter	LiCl/KCl aqueous	1.02	69	31	34	36
KM78	40% poreformer, 900°C sinter	Dip melted eutectic salt	1.06	72	28	48	24
CT115	50% poreformer, 900°C sinter	Gradual T increase	0.48	71	29	62	9
E1C	vol%s after melting	Pressed pellet	0.42		20	80	0?

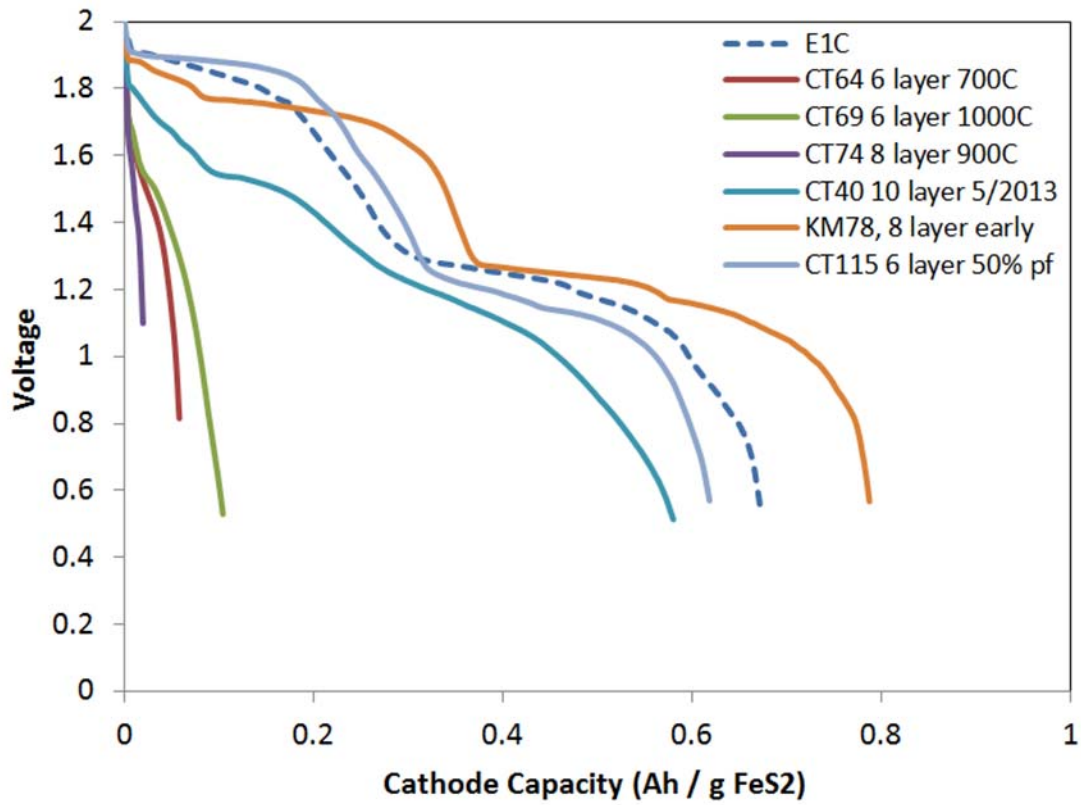

Figure 47. Voltage of single cells composed of an anode, cathode, and 1 inch diameter gelled MgO separator, compared to a pressed pellet (E1C) under a constant current load of 50 mA/cm^2

Results using a pulsed current load are shown in Figure 48, with the pellets defined in Table 5. Only one pellet was tested, and that not filled optimally. Here the tape cast ceramic pellet did not perform as well as the pressed separator pellet. However, we expect better behavior with better methods to fill the ceramic pellet with electrolyte.

.

Table 5. Poreformer tape separators tested in a pulsed current single cell battery

ID	Notes	Filling method	h (mm)	Before fill	After filling		
				Total porosity	vol% MgO	vol% elect	vol% pores
CT41	40% poreformer, 900°C sinter	LiCl/KCl aqueous	1.03	70	30	35	35
E1C	vol%s after melting	Pressed pellet	0.42		20	80	0?

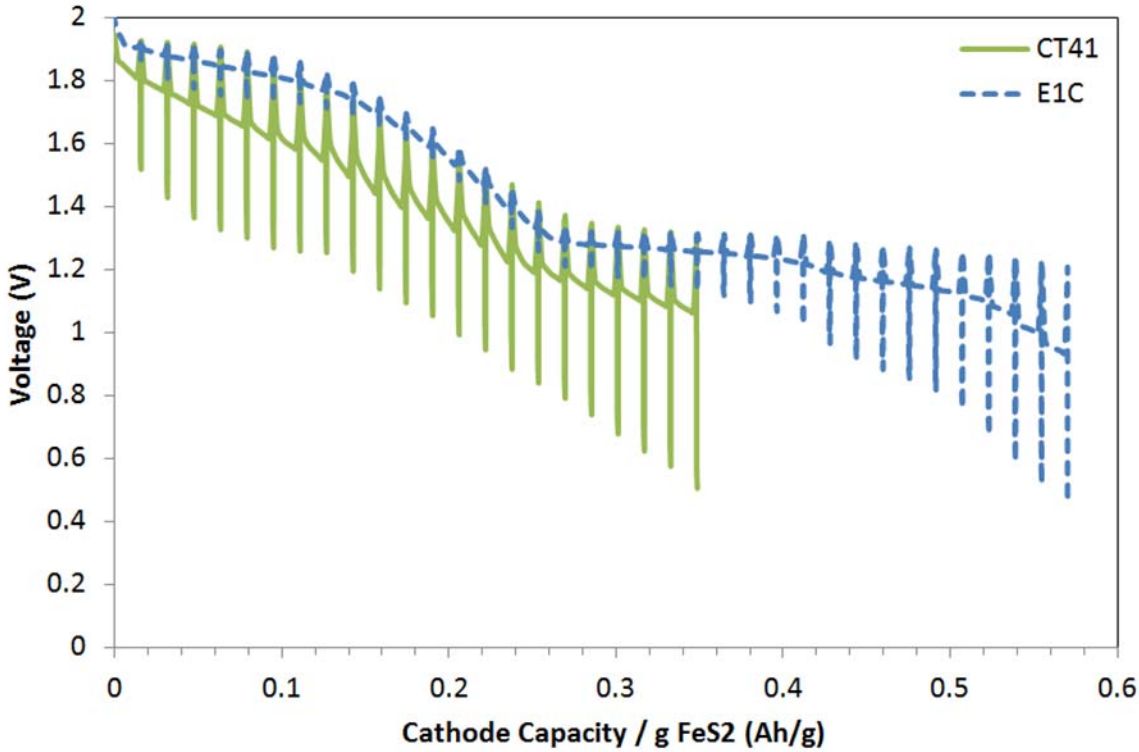

Figure 48. Voltage of single cells composed of an anode, cathode, and 1 inch diameter poreformer tape separator, compared to a pressed pellet (E1C) under a pulsed current load.

8. CONCLUSIONS

We showed that it is possible to manufacture a strong macroporous ceramic film that can be backfilled with electrolyte to form rigid separator pellets for thermal batteries. Preliminary single cell battery testing showed that the performance of ceramic separator pellets could be equal if not superior to current pressed pellets. Although, less than optimally filled with electrolyte, examples were seen that resulted in longer voltage life with comparable resistance at the critical early times.

Advantages of such a manufacturing scheme over pressing separator pellets in the conventional manner include:

1. Pellets of large diameter could be made thinner than pressed pellets
2. Pellets are rigid and are not susceptible to slippage when mechanically shocked
3. The process is amenable to scale up to produce large numbers of pellets quickly and cost effectively
4. Pellet quality is not dependent on a particular type of MgO powder, lowering Sandia's reliance on outside vendors
5. Pellets can be cut into arbitrary shapes and filled to arbitrary electrolyte content

In the following paragraphs, we will address each of these points.

With current technology, pressed pellet separators are too brittle if made thin, so battery stack heights are difficult to reduce while maintaining power output, especially for the larger diameter batteries. Although the ceramic pellets described in this report are also brittle, they are not significantly more brittle in large sheets than in small pieces. Furthermore, they gain in strength when backfilled with electrolyte, so the manufacturing steps that are most likely to result in breakage occur before stacking the pellets in a battery.

Current pressed pellets compress when the electrolyte melts, and the binder (MgO) particles rearrange until forces are balanced. These separators are subject to further particle rearrangement and compression in abnormal environments. Battery stack slippage has been observed in some shock tests, possibly because of this. Furthermore, material movement in thin separator pellets over long discharge times could lead to a short circuit between the anode and cathode and potential thermal runaways (Guidotti & Reinhardt, 2006).

The manufacturing process to create rigid ceramic separators could be done routinely at Sandia without the pitfalls of relying on commercial products and at a decreased production cost. Our examples included using a tape caster that is identical to one already installed in the Power Sources & Metrology Group. The addition of a belt furnace would drastically reduce the time of the rate-limiting step in our work, the sintering process. Cutting the pellets from tape is much faster than pressing pellets. Furthermore, note that all steps prior to backfilling with electrolyte do *not* need to be done in a dry room, which frees up valuable lab space. Like the sintering step, the process of backfilling with electrolyte could be done in large batches or in a continuous manner to increase throughput.

Furthermore, the quality of the ceramics is far less sensitive than pressed pellets to the type of MgO powder used. We used multiple lots of off-the-shelf material without detecting differences in the resulting product; thus, we believe that most materials could be used with only minor optimization steps required if the material source changed. This is in marked contrast to current pressed pellet technology that relies on specific porous qualities of MagLite S or the few other "magic" powders that can retain electrolyte and provide sufficient strength to a separator pellet once the battery is activated and the electrolyte melts.

Manufacturing rigid ceramic separators is a more agile process than pressing pellets. The tape (made in large batches) can be stacked to various heights and cut into any shape. This eliminates the need for developing and obtaining a new separator pellet die for each battery geometry. The amount of electrolyte can also be varied if desired.

We have developed unique ceramic materials with high porosity that may be useful in many other applications. We have two technical advances currently going through the Sandia patent process. That said, there is more work to be done before any of the described processes are optimized to produce battery separators. Several failures were seen in early single-cell tests (Figure 45 - Figure 48). Although better filling methods were devised after this preliminary single cell testing was completed, it is not clear at this time if electrolyte-filling was the only problem that needed correction. We are currently producing a large number of filled pellets to continue voltage testing. Furthermore, although we only tested pellets from two of our ceramic manufacturing techniques, others such as the Pickering-emulsion- and reticulated-foam-based methods show promise as well and may be worth pursuing development in the future. Other electrolyte-filling methods may work with Pickering emulsions, and smaller ppi foams may allow sufficient electrolyte retention in the reticulated foam ceramics in the future.

9. REFERENCES

Akartuna, I., Studart, A.R., Tervoort, E., Gauckler, L.J., 2008a. Macroporous Ceramics from Particle-stabilized Emulsions. Adv. Mater. 20, 4714–4718.

Akartuna, I., Studart, A.R., Tervoort, E., Gonzenbach, U.T., Gauckler, L.J., 2008b. Stabilization of Oil-in-Water Emulsions by Colloidal Particles Modified with Short Amphiphiles. Langmuir 24, 7161–7168.

Akartuna, I., Tervoort, E., Wong, J.C.H., Studart, A.R., Gauckler, L.J., 2009. Macroporous polymers from particle-stabilized emulsions. Polymer 50, 3645–3651.

Almond, D.P., West, A.R., 1983. Impedance and modulus spectroscopy of real dispersive conductors. Solid State Ionics 11, 57–64.

Amaral, L.F., Oliveira, I.R., Bonadia, P., Salomão, R., Pandolfelli, V.C., 2011. Chelants to inhibit magnesia (MgO) hydration. Ceram. Int. 37, 1537–1542.

Archie, G.E., 1942. The electrical resistivity log as an aid in determining some reservoir characteristics. Trans Aime 146, 54–62.

Arditty, S., Whitby, C.P., Binks, B.P., Schmitt, V., Leal-Calderon, F., 2003. Some general features of limited coalescence in solid-stabilized emulsions. Eur. Phys. J. E 11, 273–281.

Arora, P., Zhang, Z.J., 2004. Battery separators. Chem. Rev. 104, 4419–4462.

Aveyard, R., Binks, B.P., Clint, J.H., 2003. Emulsions stabilised solely by colloidal particles. Adv. Colloid Interface Sci. 100–102, 503–546.

Bachinger, A., Kickelbick, G., 2010. Pickering emulsions stabilized by anatase nanoparticles. Monatshefte Für Chem. - Chem. Mon. 141, 685–690.

Balberg, I., 1986. Excluded-volume explanation of Archie's law. Phys. Rev. B 33, 3618–3620.

Bandyopadhyay, G., R. B. Swaroop, and J. E. Battles, 1982. J. Electrochem. Soc. 128, 2187.

Barsoukov, E., Macdonald, J.R. (Eds.), 2005. Impedance Spectroscopy: Theory, Experiment, and Applications, 2nd ed. Wiley-Interscience.

Binks, B.P., Lumsdon, S.O., 2001. Pickering Emulsions Stabilized by Monodisperse Latex Particles: Effects of Particle Size. Langmuir 17, 4540–4547.

Binks, B.P., Whitby, C.P., 2004. Silica Particle-Stabilized Emulsions of Silicone Oil and Water: Aspects of Emulsification. Langmuir 20, 1130–1137.

Brandriss, S., Margel, S., 1993. Synthesis and characterization of self-assembled hydrophobic monolayer coatings on silica colloids. Langmuir 9, 1232–1240.

Chen, X., Liu, K., He, P., Zhang, H., Fang, Y., 2012. Preparation of Novel W/O Gel-Emulsions and Their Application in the Preparation of Low-Density Materials. Langmuir 28, 9275–9281.

Chuanuwatanakul, C., Tallon, C., Dunstan, D.E., Franks, G.V., 2011. Controlling the microstructure of ceramic particle stabilized foams: influence of contact angle and particle aggregation. Soft Matter.

Colombo, P., Degischer, H.P. 2010. Highly porous metals and ceramics. Materials Science and Technology 26, 1145-1158.

Dullien, F.A.L., 1975. Single phase flow through porous media and pore structure. Chem. Eng. J. 10, 1–34.

Finkle, P., Draper, H.D., Hildebrand, J.H., 1923. The theory of emulsification. J. Am. Chem. Soc. 45, 2780–2788.

Fruhwirth, O., Herzog, G.W., Hollerer, I., Rachetti, A., 1985. Dissolution and hydration kinetics of MgO. Surf. Technol. 24, 301–317.

Gonzenbach, U.T., Studart, A.R., Tervoort, E., Gauckler, L.J., 2006. Ultrastable Particle-Stabilized Foams. Angew. Chem. Int. Ed. 45, 3526–3530.
Guidotti, R.A., F. W. Reinhardt, 1996. . Proc. 37th Power Sources Conf. 251.
Guidotti, R.A., Reinhardt, F.W., Dai, J., Reisner, D.E., 2006. Performance of thermal cells and batteries made with plasma-sprayed cathodes and anodes. J. Power Sources 160, 1456–1464.
Gurevitch, I., Silverstein, M.S., 2010. Polymerized pickering HIPEs: Effects of synthesis parameters on porous structure. J. Polym. Sci. Part Polym. Chem. 48, 1516–1525.
Haase, M.F., Grigoriev, D., Moehwald, H., Tiersch, B., Shchukin, D.G., 2011. Nanoparticle Modification by Weak Polyelectrolytes for pH-Sensitive Pickering Emulsions. Langmuir 27, 74–82.
I. Akartuna, E.T., 2009. Macroporous polymers from particle-stabilized emulsions. Polymer 50, 3645–3651.
Imhof, A., Pine, D.J., 1997. Ordered macroporous materials by emulsion templating. Nature 389, 948–951.
Kumari, L., Li, W.Z., Vannoy, C.H., Leblanc, R.M., Wang, D.Z., 2009. Synthesis, characterization and optical properties of Mg(OH)2 micro-/nanostructure and its conversion to MgO. Ceram. Int. 35, 3355–3364.
Lide, D., 1996. CRC Handbook of Chemistry and Physics, 77th ed. CRC Press, Boca Raton.
MacMullin, R.B., Muccini, G.A., 1956. Characteristics of porous beds and structures. Aiche J. 2, 393–403.
Mejias, J.A., Berry, A.J., Refson, K., Fraser, D.G., 1999. The kinetics and mechanism of MgO dissolution. Chem. Phys. Lett. 314, 558–563.
Merwe, E.M. van der, Strydom, C., Botha, A., 2004. Hydration of medium reactive industrial magnesium oxide with magnesium acetate. J. Therm. Anal. Calorim. 77, 49–56.
Michael Scheffler, Colombo, P., 2005. Cellular Ceramics. Wiley-VCH Verlag GmbH & Co., Weinheim, Germany.
Neirinck, B., Fransaer, J., Van der Biest, O., Vleugels, J., 2009. A novel route to produce porous ceramics. J. Eur. Ceram. Soc. 29, 833–836.
Nettleship, I., 1996. Applications of Porous Ceramics. Key Eng. Mater. 122-124, 305–324.
Orazem, M.E., Tribollet, B., 2008. An integrated approach to electrochemical impedance spectroscopy. Electrochimica Acta 53, 7360–7366.
Park, B.J., Pantina, J.P., Furst, E.M., Oettel, M., Reynaert, S., Vermant, J., 2008. Direct Measurements of the Effects of Salt and Surfactant on Interaction Forces between Colloidal Particles at Water−Oil Interfaces. Langmuir 24, 1686–1694.
Paunov, V.N., 2003. Novel Method for Determining the Three-Phase Contact Angle of Colloid Particles Adsorbed at Air−Water and Oil−Water Interfaces. Langmuir 19, 7970–7976.
Phillips, V.A., Kolbe, J.L., Opperhauser, H., 1977. Effect of pH on the growth of Mg(OH)2 crystals in an aqueous environment at 60°C. J. Cryst. Growth 41, 228–234.
Pickering, S.U., 1907. Emulsions. J. Chem. Soc. Trans. 91, 2001.
Pokrovsky, O.S., Schott, J., 2004. Experimental study of brucite dissolution and precipitation in aqueous solutions: surface speciation and chemical affinity control. Geochim. Cosmochim. Acta 68, 31–45.
Rice, R.W., 1998. Porosity of Ceramics. Marcel Dekker, New York, NY.
Roberts, C.C., n.d. Highly porous ceramic foams from magnesium oxide stabilized Pickering emulsions. Langmuir.

Roy-Perreault, A., H. Kueper, B., Rawson, J., 2005. Formation and stability of polychlorinated biphenyl Pickering emulsions. J. Contam. Hydrol. 77, 17–39.
San-Miguel, A., Behrens, S.H., 2012. Influence of Nanoscale Particle Roughness on the Stability of Pickering Emulsions. Langmuir 28, 12038–12043.
Song, M.-K., Park, S., Alamgir, F.M., Cho, J., Liu, M., 2011. Nanostructured electrodes for lithium-ion and lithium-air batteries: the latest developments, challenges, and perspectives. Mater. Sci. Eng. R Reports 72, 203–252.
Studart, A.R., Gonzenbach, U.T., Tervoort, E., Gauckler, L.J., 2006. Processing Routes to Macroporous Ceramics: A Review. J. Am. Ceram. Soc. 89, 1771–1789.
Sturzenegger, P.N., Gonzenbach, U.T., Koltzenburg, S., Gauckler, L.J., 2012. Controlling the formation of particle-stabilized water-in-oil emulsions. Soft Matter.
Vandebril, S., Vermant, J., Moldenaers, P., 2010. Efficiently suppressing coalescence in polymer blends using nanoparticles: role of interfacial rheology. Soft Matter 6, 3353.

DISTRIBUTION (ELECTRONIC COPIES)

1	MS0899	Technical Library	9536
1	MS0359	D. Chavez, LDRD Office	1911
1	MS0161	Legal Technology Transfer Center	11500
1	MS0346	Lisa Mondy	1512
1	MS0346	Christine Roberts	1512
1	MS0346	Anne Grillet	1512
1	MS0346	Melissa Soehnel	1512
1	MS0346	David Barringer	1512
1	MS0346	Tracie Durbin	1514
1	MS0958	Chris Diantonio	1816
1	MS0958	Tom Chavez	1816
1	MS1411	Paul Clem	1816
1	MS0613	David Ingersoll	2546
1	MS0613	Thomas Wunsch	2546
1	MS0958	Lindsey Hughes	1835
1	MS0888	James McElhanon	1835
1	MS0958	Lindsey Evans	1815
1	MS1349	William Hammetter	1815
1	MS0885	Mark F. Smith	1830
1	External	Stephanie Fitchett	

Sandia National Laboratories